Fundamentals of Liquid Metal Foams and Emulsions

by

Najam Ul Hassan Shah

A Dissertation Presented in Partial Fulfillment
of the Requirements for the Degree
Doctor of Philosophy

Approved September 2022 by the
Graduate Supervisory Committee:

Konrad Rykaczewski, Co-Chair
Robert Wang, Co-Chair
Patrick Phelan
Matthew D. Green
Beomjin Kwon

ARIZONA STATE UNIVERSITY

May 2023

ABSTRACT

Gallium based room-temperature liquid metals (LMs) have special properties such as metal-like high thermal conductivity while in the liquid state. They are suitable for many potential applications, including thermal interface materials, soft robotics, stretchable electronics, and biomedicine. However, their high density, high surface tension, high reactivity with other metals, and rapid oxidation restrict their applicability. This dissertation introduces two new types of materials, LM foams, and LM emulsions, that address many of these issues. The formation mechanisms, thermophysical properties, and example applications of the LM foams and emulsions are investigated.

LM foams can be prepared by shear mixing the bulk LM in air using an impeller. The surface oxide layer is sheared and internalized into the bulk LM as crumpled oxide flakes during this process. After a critical amount of oxide flakes is internalized, they start to stabilize air bubbles by encapsulating and oxide-bridging. This mechanism enables the fabrication of a LM foam with improved properties and better spreadability.

LM emulsions can be prepared by mixing the LM foam with a secondary liquid such as silicone oil (SO). By tuning a few factors such as viscosity of the secondary liquid, composition, and mixing duration, the thermophysical properties of the emulsion can be controlled. These emulsions have a lower density, better spreadability, and unlike the original LM and LM foam, they do not induce corrosion of other metals.

LM emulsions can form by two possible mechanisms, first by the secondary liquid replacing air features in the existing foam pores (replacement mechanism) and second by creating additional liquid features within the LM foam (addition mechanism). The latter mechanism requires significant oxide growth and therefore requires presence of oxygen in

the environment. The dominant mechanism can therefore be distinguished by mixing LM foam with the SO in air and oxygen-free environments. Additionally, a comprehensive analysis of foam-to-emulsion density change, multiscale imaging and surface wettability confirm that addition mechanism dominates the emulsion formation. These results provide insight into fundamental processes underlying LM foams and emulsions, and they set up a foundation for preparing LM emulsions with a wide range of fluids and controllable properties.

DEDICATION

I dedicate this dissertation to my family and parents for supporting my learning journey.

"Seek knowledge from the cradle to the grave."

- Prophet Muhammad (peace be upon him)

ACKNOWLEDGMENTS

First, I thank Dr. Robert Wang and Dr. Konrad Rykaczewski for being my Ph.D. advisors and for your tremendous support throughout my Ph.D. program. I am extremely grateful for being accepted as your student and appreciate your patience and guidance during these formative years in my research career. I enjoyed working in your groups and having two complementary sets of expertise that shaped my approach to research. I thank my committee members, Dr. Patrick Phelan, Dr. Matthew Green and Dr. Beomjin Kwon. I extend my gratitude to all my lab mates, both past and present, for being incredibly talented researchers and amazing people to work with: especially Dr. Wilson Kong for mentoring me like an elder brother during most of my PhD research, Astha Uppal, Dr. Praveen Kotagama, Dr. Akshay Phadnis, Dr. Kenneth Manning, Ashish Rana, Yanan Zhang, Shreyas Kanetkar and Nathan Casey. Outside of ASU, I thank Dr. Michael Dickey (the liquid metal expert) and his team from NCSU for their contributions to our LM foams and Emulsion formation mechanism papers.

I am highly grateful to the Fulbright-HEC scholarship program for fully funding my PhD studies and to my employer, the University of Engineering and Technology Taxila, Pakistan for granting my study leave to pursue my PhD program. For research funding, I acknowledge the support by Semiconductor Research Corporation (#2017-PK-2787) and National Science Foundation (grant 2032415). I thank Arizona State University Graduate College and their funding sources for awarding out-of-state tuition waiver through out my degree program.

I thank my wife for being supportive, encouraging, and uplifting during my time in graduate school and caring for our kids at home. I also thank my six-year-old daughter,

Aleha, for being so supportive and compassionate; I am highly indebted for the precious family time that I stole from your pre- and early school age. Lastly, I thank my parents, for being so supportive and kind throughout my life. I am indebted to your exemplary parenting and your perseverance for ensuring my early and higher education despite many challenges.

As a student of ASU, I acknowledge that the Tempe campus sits on the ancestral homelands of those American Indian tribes that have inhabited this place for centuries, including the Akimel O'odham (Pima) and Pee Posh (Maricopa) peoples.

I also thank all my friends both inside and outside ASU as well as communities at Pakistan Students Association, Almehdi center and IEFAZ for providing a support network and opportunities to enjoy my time outside of ASU. Thank you all!

TABLE OF CONTENTS

Page

LIST OF FIGURES ix

NOMENCLATURE xiii

CHAPTER

1. INTRODUCTION.....1

1.1. Gallium Based Liquid Metals 1

1.1.1. Motivation.....1

1.1.2. Liquid Metal Properties and Applications 2

1.2. Fabricating LM-materials with Tunable Properties 4

1.2.1. Mixing Other Materials to Liquid Metals 4

1.2.2. Challenges in Incorporating Other Fluids into LM.....6

1.3. Formation of LM Foams and Liquid-in-LM Emulsions.....8

2. OXIDE MEDIATED MECHANISM OF FOAM FORMATION BY SHEAR MIXING IN AIR 12

2.1. Fabrication of LM Foams 13

2.2. Onset of Foam Formation 15

2.2.1. Structural Characterization (Composition of LM Foams) 15

2.2.2. Density of LM Foams 17

2.3. Thermal and Rheological Properties of LM Foams.....18

2.4. Mechanism of Foam Formation 21

2.5. Conclusion.....22

3. GALLIUM-OXIDE STABILIZED OIL-IN-LIQUID METAL EMULSIONS 24

CHAPTER Page

3.1. Fabrication of LM Emulsions 24

3.2. Effect of Viscosity and Mixing Time on Emulsion Formation 26

3.3. Phase Inversion of Oil-in-LM Emulsion upon Extensive Mixing.....28

3.4. Effect of Volumetric Content of SO on Oil-in-LM Emulsion.....29

3.5. Preventing Corrosion of Aluminum Substrates 31

3.6. Conclusion.....33

4. EMULSION FORMATION MECHANISM 36

4.1. Two Mechanisms of Liquid-in-LM Emulsions Formation 37

4.1.1. Description 37

4.1.2. Theoretical LM Foam-to-Emulsion Density Difference.....38

4.2. Identifying Underlying Mechanism for Formation of Liquid-in-LM Emulsion 41

4.2.1. Analysis of Density of Silicone Oil and LM Foam Mixed in Air and Nitrogen Environments 41

4.2.2. Surface Wettability and Multiscale Imaging of the Silicone Oil Mixed with the LM Foam in Air and Nitrogen Environments 44

4.3. Suitability of the Silicone Oil and LM FoamTmixtures for Thermal Interface Materials 48

4.3.1. Prevention of LM-induced Embrittlement of Aluminum Foil.....48

4.3.2. Thermal Conductivity 49

4.4. Conclusion.....51

5. FUTURE WORK 53

CHAPTER Page

5.1. Summary of Dissertation 53

5.2. On-going Research.....55

5.3. Future Directions.....57

5.4. Preliminary Experiments of Using Oleic Acid as Surfactant 57

REFERENCES 62

APPENDIX

A SUPPORTING INFORMATION FOR CHAPTER 2.....71

B SUPPORTING INFORMATION FOR CHAPTER 3.....80

C SUPPORTING INFORMATION FOR CHAPTER 4.....83

BIOGRAPHICAL SKETCH.....89

LIST OF FIGURES

Figure Page

1.1: Comparison of Pure LM Properties, Processibility, and Applications with Proposed Materials (LM Foams and Emulsions) 2

1.2: An Overview of Important Properties of Gallium Based Liquid Metals 3

1.3: Plot of Thermal Conductivity against Density of Different LM-materials Showing Research Gap 6

1.4 Buoyancy Driven Escape of Injected Fluids to the Top Surface of LM (A) Air Bubble, (B) Silicone Oil Bubble 7

1.5: Schematic Representation of Various Breakdown Processes in Emulsions 8

1.6: Shear-mixing of Bulk LM in Air for Formation of Stable LM Foam 9

1.7: Liquid-in-LM Emulsion Formation by Mixing Secondary Liquid with LM Foam 9

1.8: Two Possible Routes Of Secondary Liquid Incorporation Into The LM Foam 10

2.1: (A) Schematic of Gallium Foam Fabrication by Shear-mixing of Liquid Gallium in Air; (B) Surface Waves Created by High-speed Mixing, (C) Gallium-oxide Islands on the Surface of the Stirred LM; (D) Focused Ion Beam Image Showing Oxide-islands Generated Through Ion Ablation on the Surface of LM in Vacuum. 14

2.2: SEM Images of Gallium Foam Cross-sections Processed at Different Mixing Times (0-120 Minutes) 16

2.3: SEM Image of a Crumpled Gallium Oxide Internalized in the Bulk LM 17

2.4: Plot of Gallium Foam Density as a Function of Mixing Time 18

2.5: Plot of Gallium Foam Thermal Conductivity as a Function of Mixing Time 19

Figure Page

2.6: Plot of Viscosity and Storage Modulus of Gallium Foam as a Function of Mixing Time 20

2.7: Schematic of Liquid Gallium Foaming Mechanisms: A) Oxide Flake Accumulation During Shear Mixing and B) Oxide-mediated Air Capsule Stabilization and Accumulation. 22

3.1: (A) Overview of Shear-mixing Based Fabrication of LM-in-oil Emulsions and Oil-in-LM Emulsions and (B) Cross-sectional SEM Images of LM-based Foam Before and after Mixing with Silicone Oil (SO) Which Results in the Formation of Oil-in-LM Emulsion. 25

3.2: (A) Optical Images of LM-in-Oil Emulsions Made with 10 to 10,000 cst Viscosity SOs (20:80 SO:LM Volume Ratio and 30 Minutes of Mixing), (B) Optical Images of Oil-In-LM Emulsion Cross Sections Made with 10 to 10,000 cst Viscosity SOs (20:80 SO:LM Foam Volume Ratio and 30 Minutes of Mixing) 27

3.3: (A) Illustrative Images and Schematics Showing Phase Inversion of Oil-in-LM Back into LM-in-Oil Emulsions Upon Excessive Mixing, and (B) Illustrative Processing Map Showing the Oil-in-LM Formation Window and Phase Inversion Regions (20:80 SO:LM Foam Volumetric Ratio, 120 rpm Manual Shear Mixing). 29

3.4: (A) SEM Micrographs of Oil-in-LM Emulsions Cross-sections Made with 10 cst Viscosity SO with SO:LM Foam Volumetric Ratio Ranging from 10:90 to 40:60, (B) Plot of the Effective Thermal Conductivity Against the SO Volume Percentage for Oil-in-LM Emulsions 30

Figure Page

3.5: Corrosion Protection Characteristics of Oil-In-LM Emulsions (A) Representative Images of Aluminum Foil Before and after 24-hour Contact Under .1 MPa Pressure with LM Foam and Oil-in-LM Emulsion (40:60 SO:LM Foam), (B) Bar Plot Showing Corrosion Protection Ability of 10 cst Oil-in-LM Emulsions Made with Varying Oil Content (Total 20 Tests Were Performed for Each Composition), (C) Schematic Illustrating the Mechanism of Aluminum Corrosion Protection under Compression: Wetting of the Exterior of the Emulsions by a Thin Film of SO, and (D) Images of 1 Microliter Water Droplets Placed on LM Foam and on the 40:60 Oil-in-LM Emulsion. 32

4.1: Schematics of Possible Emulsion Formation Mechanisms: (A) Air Replacement by the Secondary Liquid (S), Exemplified as (B) Air Replacement in Open-cell and (C) Closed-cell Geometrical Features; (D) Secondary Liquid Forming Additional Closed-cell Geometrical Features in LM Foam, Exemplified as (E) Formation of Liquid-filled Cavities by Surface Wave Cresting. 38

4.2: Schematics and Example Images of LM Foam and Silicone Oil (SO) Mixing in (A) an Air (I.E., the Emulsion) and (B) Nitrogen Environment; (C) the Density of the LM Materials Resulting from the Two Mixing Processes with Varying Input Volumetric Ratios of SO and LM Foam. 42

4.3: Mixing of LM Foam with Hydrogen Peroxide in (A) Air and in a (B) Nitrogen Environment 44

Figure Page

4.4: Water Contact Angles Measured on the Surfaces of the LM Foam and Its Mixtures with Silicone Oil Made in an Air (I.E., the Emulsion) or Nitrogen Environment as a Function of the Silicone Oil and The LM Foam Volumetric Mixing Ratio..... 45

4.5: Multiscale Optical and Cryo-FIB-SEM Surface and Cross-Sectional Images of (A) the Bare LM Foam and (B & C) the LM Foam Mixed with Silicone Oil (SO) in (B) Nitrogen and (C) Air Environments. 47

4.6: Photographs of Pristine Aluminum Foils and Those after 24-hour Exposure to (A) Mixed-in-Air Silicone Oil-in-LM Emulsion and the (B) LM Foam Mixed with the Silicone Oil in Nitrogen Environment..... 49

4.7: The Effective Thermal Conductivity of the Bare LM Foam and the LM Foam Mixed with Silicone Oil in Nitrogen and Air Environments. 50

5.1: Foaming of LM using Decomposition Agents 56

5.2: Using Oleic Acid as Surfactant: Mixing LM Foam with SO and OA in Air (A-C), and Nitrogen (D-F) Environments, and (G-I) Mixing Pure LM with SO and OA in Air..... 49

NOMENCLATURE

Symbol	**Description**
ASTM	American Society of Testing Materials
eGaIn	Eutectic gallium indium
eGaInSn	Eutectic gallium indium tin (also known as Galinstan)
Ga	Gallium
H_2O_2	Hydrogen peroxide
k	Thermal conductivity
k_{eff}	Effective thermal conductivity
LM	Liquid Metal
OA	Oleic acid
SO	Silicone oil
SEM	Scanning electron microscope
TIM	Thermal interface materials

CHAPTER 1

INTRODUCTION

1.1. Gallium Based Liquid Metals

1.1.1. Motivation

Gallium (Ga) and its eutectic alloys (eGaIn and eGaInSn), also collectively known as Ga-based liquid metals (LMs), have a melting point close to or below room temperature (29℃, 15.5℃, and 10.6℃ respectively).[1] These special materials are liquid at room temperature, but at the same time possess metallic characteristics such as good electrical and thermal conductivities. Although mercury (Hg) has been the only well-known LM for decades due to its applications in liquid thermometers and barometers, its toxicity and high vapor pressure restrict its continued application.[2] Unlike Hg, Ga and its alloys are non-toxic and have a negligible vapor pressure. They have low viscosity and considerable thermal and electrical conductivity. They are suitable for many potential applications, including thermal interface materials (TIMs),[3,4] soft robotics,[5] stretchable electronics,[6,7] and biomedicine.[8–10]

However, some issues restrict LMs' applicability, such as their high density, high surface tension, high reactivity with other metals, and rapid oxidation.[1] Despite their many potential uses due to their unique properties, their real-life application is still limited to a few areas, such as thermometers or select thermal interface material (TIM) applications. For example, LM's high cohesive density and surface tension make it difficult to form different shapes or apply them to different substrates. Their reactivity with other metals causes corrosion and embrittlement, which imparts physical damage to the system. Due to rapid oxidation, LMs form a thin oxide film (1-3 nm thickness) which causes abrupt and

unpredictable changes in their rheology and adhesion. These phenomena make it challenging to handle the LMs and complicates industrial manufacturing processes.

This thesis aims to address these challenges by augmenting liquid metal properties by adding secondary fluids (gas or liquids) to the LMs. This will introduce two new materials: LM foams and emulsions; these materials exhibit improved properties, higher processability, and broader scope of applications (Figure 1.1). The following sections will discuss fundamental challenges and the proposed path of this research.

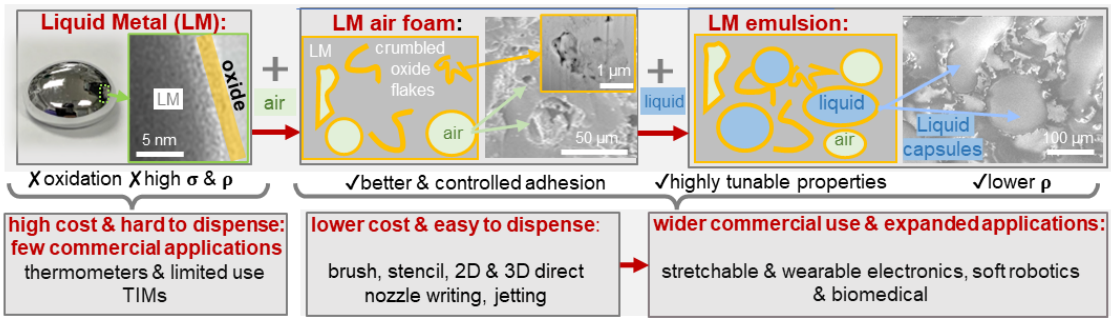

Figure 1.1: Comparison of pure LM properties, processibility, and applications with proposed materials (LM foams and emulsions)[9,11,12]

1.1.2. Liquid Metal Properties and Applications

Liquid metals possess special properties, not commonly found in other materials (Figure 1.2). Unlike other fluids, which are poor conductors of heat or electricity, Ga and its alloys exhibit high thermal (25-30 W m^{-1} K^{-1}) and electrical conductivity (0.34 - 0.38 × 10^5 S cm^{-1} in their liquid state. This makes them suitable for many applications in thermal management and soft-stretchable electronic devices.

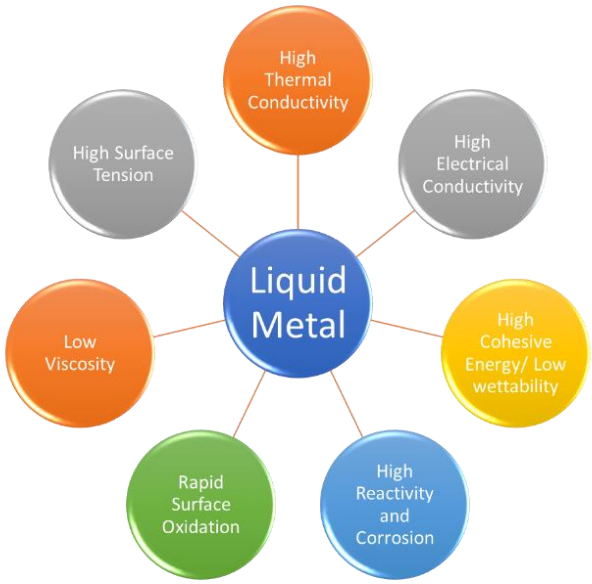

Figure 1.2: An overview of important properties of gallium based liquid metals

The LMs have a much higher density (5.9 – 6.4 g/cm^3) than other fluids, six times that of water. This may be useful in some applications, but it can be undesirable in mobile applications and wearable devices.

The surface tension of gallium and its alloys ranges from 587-724 mN m^{-1}, up to 10 times that of water (72.7 mN^{-1} m). This high surface tension originates from high cohesive energy density due to metallic bonds between the LM atoms. This results in the non-wetting characteristic of LM with other surfaces and substrates. When dispensed on other substrates, LM tends to bead up in a spherical shape rather than forming useful shapes such as thin wires or sheets.

Gallium-based LMs are characterized by low viscosity (1.69-2.5 cP), which is close to that of water (1 cP). This makes LMs ideal for applications in soft, stretchable, and flexible devices. However, in ambient conditions, the rheology of LMs is dominated by the rapidly forming oxide skin which is responsible for its viscoelastic behavior.

The LMs readily oxidize, even at reduced oxygen partial pressure, to form a thin oxide film (1-3 nm thickness) mainly consisting of β-gallium oxide (Ga_2O_3). The oxide skin behaves solid-like, adding yield stress to the fluid core. This makes it possible to stabilize LMs into different shapes and support patterning and deposition techniques. This also imparts viscoelastic behavior to the LMs and increases nominal viscosity up to two orders of magnitude. However, the growth of oxide skin is uncontrolled, resulting in uncertainty in LM properties at any given time, thereby making its handling and industrial manufacturing processes difficult.

LMs are also reactive with most metals, and cause corrosion and embrittlment.[13] Liquid Ga and its alloys form intermetallic compounds and cause corrosion to typical metal substrates used in chip cooling (such as $CuGa_2$ with copper).[14,15] They penetrate into grain boundaries of aluminum, one of the most common heat sink materials, resulting in embrittlement and severe material damage.[16] With silver, Ga reacts spontaneously to form Ag_2Ga alloy with a nanoscale needle-like morphology.[17] These reactions may unexpectedly change the LM properties and impart physical damage to the system.

For the reliable design of industrial processes, it is essential to limit the reactivity and gain precise control over the viscoelastic and other properties of LMs. Moreover, it is important that the LM's properties are easy to modify and tunable on demand to fit the needs of different applications. This can be achieved by mixing LMs with other materials such as solid additives or polymeric fluids.

1.2. Fabricating LM-materials with Tunable Properties

1.2.1. Mixing Other Materials to Liquid Metals

One way to control the viscoelastic properties of LMs is by adding solid fillers. Usually, highly conductive fillers are used for TIM application, such as copper,[18] silver,[19–21] diamond,[22] tungsten,[4] silicon carbide,[23] and graphene[24] etc. For example, Kong et al.[4,23] achieved up to a three-fold increase in thermal conductivity of liquid eGaInSn by incorporating 40% by volume of tungsten or SiC particles. This method results in the formation of LM-solid composites, which have a higher viscosity, better wettability, and higher thermal conductivity. However, this also increases their density and cost, and does not eliminate the risk of LM embrittlement of other materials.

To circumvent the embrittlement issue, researchers dispersed LM into silicone grease or a polymeric matrix resulting in the formation of LM-polymer composites or greases.[25] These materials are electrically insulating, making them good for on-chip TIM applications. However, their thermal conductivity is significantly reduced due to the insulating matrix material and poor contact between the LM droplets. To reach higher thermal conductivities, it is necessary to establish thermal percolation pathways between LM particles. This may require additional processing and complicated fabrication techniques.[25–28]

In either of the above two approaches, some properties are improved at the cost of degrading others. To increase the thermal conductivity (desired), the density must generally be increased (undesired). Similarly, thermal conductivity is significantly degraded when trying to eliminate LM-embrittlement. This represents the two opposite ends on the thermal conductivity-density plot (Figure 1.3), leaving a gap yet to be filled by a new type of material. This gap can be filled by the LM foams and liquid-in-LM emulsions that are investigated in this research.

LM foam and liquid-in-LM emulsion can be prepared by adding other fluids (gas or liquid fillers) to the LM. However, to realize these materials, several challenges need to be addressed.

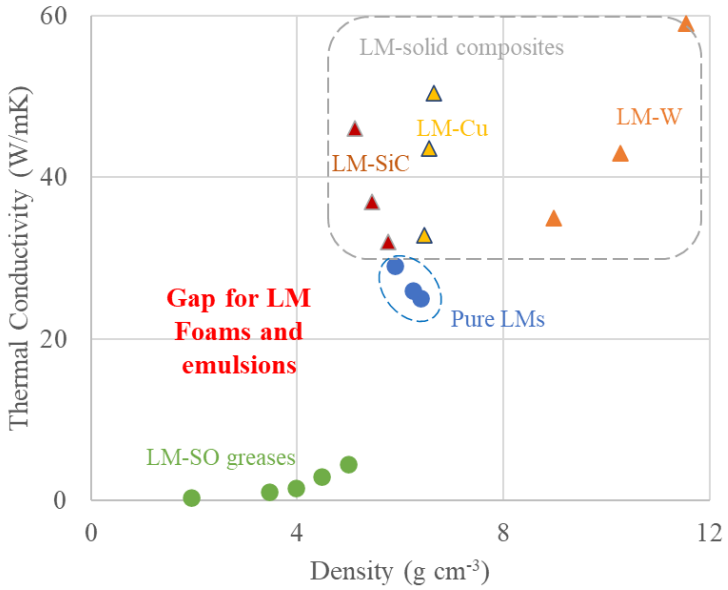

Figure 1.3: Thermal conductivity-density plot of different LM-materials showing research gap

1.2.2. Challenges in Incorporating Other Fluids into LM

Although fabrication of LM-solid or LM-polymer composites is quite common, [29] no work has been dedicated to fabricate LM foams or liquid-in-LM emulsions until recently.[4,30–34] Several potential challenges may be outlined from a review of general literature (such as oil-water emulsions) [35–37] or from observing basic experiments of mixing LM with other liquids as described below.

Pure LMs are immiscible with other liquids and do not entrain air bubbles. When mixed with other liquids such as silicone oil, LMs tend to disperse in the form of droplets due to their high cohesive energy density. Oxide shells stabilize these LM droplets due to

the presence of dissolved oxygen in the liquids. Thus, LMs have a preferred arrangement in which they mix; inverting this preferred arrangement may not be easy. To overcome this challenge, the cohesive energy of the LMs must be reduced.

If another fluid or a gas bubble is injected into the bulk LM, it tries to escape as soon as introduced (see examples in Figure 1.4). The density difference creates a buoyancy force that pushes the fluid bubble up, and it escapes to the top surface of the LM. The low viscosity of the LM supports this escape of the secondary fluid. To overcome this challenge, it is necessary to overcome the barrier of density difference and increase viscosity to trap fluid bubbles.

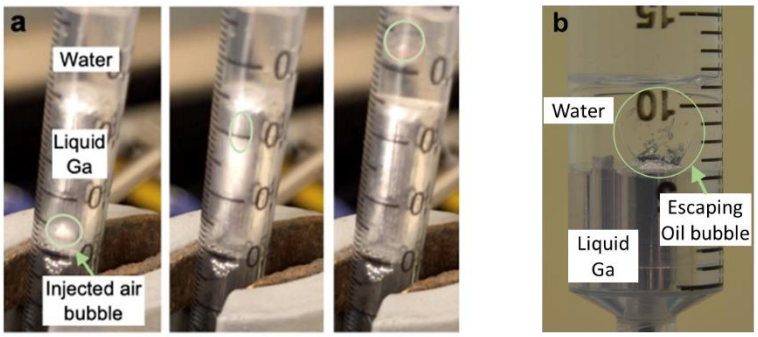

Figure 1.4 Buoyancy driven escape of injected fluids to the top surface of LM (a) air bubble, (b) Silicone oil bubble

The LM foam and liquid-in-LM emulsions may also suffer from breakdown processes observed in other emulsions (Figure 1.5), such as coalescence, phase inversion, Ostwald ripening, flocculation etc.[38] For example, the individual air or liquid bubbles dispersed in the bulk LM may combine to form larger bubbles (coalescence). It is necessary to stabilize the internal liquid-LM interfaces to inhibit such breakdown processes.

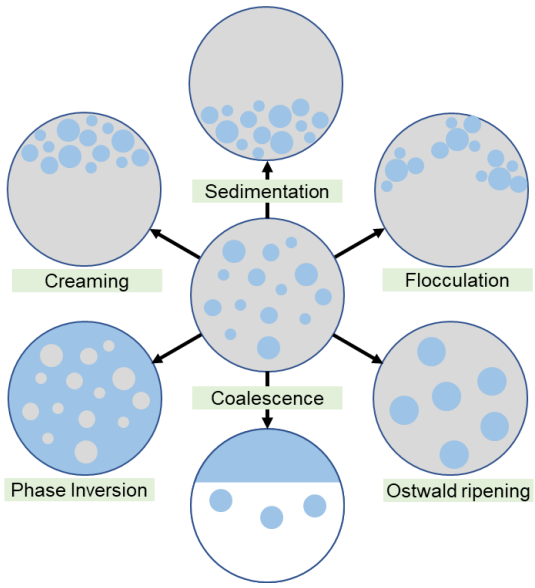

Figure 1.5: Schematic Representation of various breakdown processes in emulsions [38]

In the next section, I will discuss the way to overcome these challenges and summarize the remaining chapters of my dissertation.

1.3. Formation of LM Foams and Liquid-in-LM Emulsions

To stabilize LM foams and emulsions, LM properties must be tuned in a favorable way (low density and high viscosity). 'Emulsifying agents' must be introduced to stabilize air or liquid bubbles. The native gallium oxide skin on LM surface may provide an easy way to achieve these targets.

As mentioned earlier, LMs rapidly oxidize in ambient conditions and develop a native oxide skin of 1-3 nm thickness. This oxide skin alters LM properties in many ways: augments effective surface tension, increases viscosity by introducing viscoelasticity, adds wettability, and allows incorporation of other medium such as solid fillers. The oxide skin behaves elastically with a yield stress value, and it may be ruptured by shearing with

sufficient force. This would expose a fresh LM surface, which would rapidly oxidize to form a new oxide skin. Repeated breakage-and-formation of oxide would generate oxide flakes that accumulate in the bulk LM. These oxide flakes may favorably alter the LM properties and act as emulsifying and bridging agents to stabilize air bubbles in LM foam.

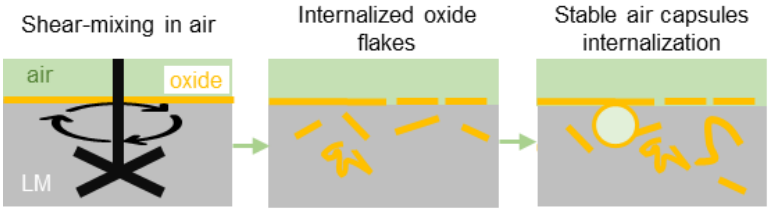

Figure 1.6: Shear-mixing of bulk LM in air for formation of stable LM-air-foam

Room-temperature LM foam can be prepared by shear mixing the bulk LM in air (as shown in Figure 1.6). In this process, specific quantities of LM are taken in a container and stirred at a higher speed using an impeller. The rotating impeller continues to shear and internalize crumpled oxide flakes into the LM, increasing LM's viscosity and oxide content. Air bubbles are trapped in the LM due to surface perturbations and stabilized by the oxide flakes and rapidly forming oxide shells around these bubbles. This foam has a lower density, higher viscosity, and can be easily spread to different surfaces. Further details of the fundamental mechanism of LM-foam formation and a detailed investigation of its processing-structure-property relationship is discussed in Chapter 2.

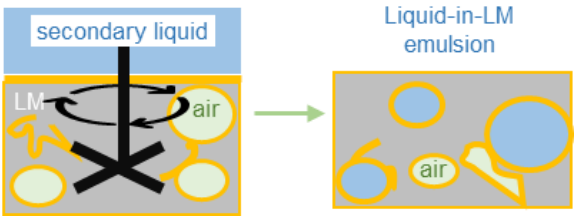

Figure 1.7: Liquid-in-LM emulsion formation by mixing secondary liquid with LM-foam

LM emulsions can be prepared by mixing the LM foam with a secondary liquid such as silicone oil (as shown in Figure 1.7). Unlike the pure LM which disperses into smaller droplets when mixed with a secondary liquid, the LM foam can internalize secondary liquid resulting in liquid-in-LM emulsion. The oxide and foam features in the LM-foam stabilize the droplets of secondary liquid. By tuning a few factors such as viscosity of the secondary liquid, composition, and mixing duration, the thermophysical properties of the emulsion can be controlled. These emulsions have a lower density, better spread-ability, and do not induce corrosion of other metals such as is the case with the original LM and LM foam. Chapter 3 presents a detailed investigation of the stability of these emulsions through a range of processing times and the viscosity of a secondary fluid and the impact of these parameters on the materials' structure and thermal property relationships.

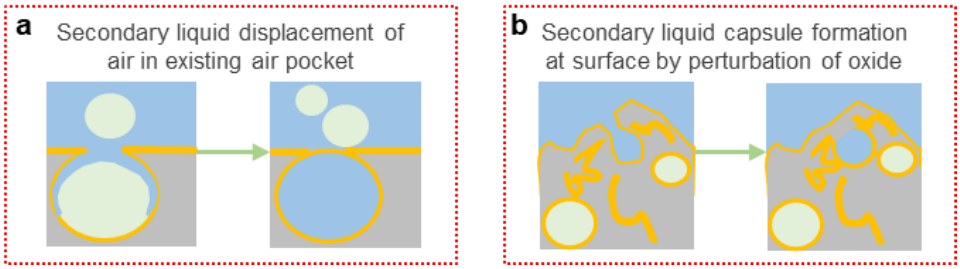

Figure 1.8: Two possible routes of secondary liquid incorporation into the LM-foam

The incorporation of secondary liquid into the LM could occur in two possible ways (as shown in Figure 1.8). First, the emulsion might form through the secondary liquid displacement of air within existing features within the foam (i.e., pores, rupturing pockets) named as the "replacement mechanism". Second, gallium oxide-enclosed secondary liquid

capsules can form during perturbation of the oxide at the two bulk liquid interfaces throughout the mixing process, named as the “addition mechanism”. Additional oxide could also form as the capsules are internalized. The oxide would mechanically stabilize the internal secondary liquid-LM interface, while the oxide flakes prevent the buoyancy-driven escape of the capsules by mechanically bridging the space in between capsules. The latter mechanism requires significant oxide growth and therefore requires presence of oxygen in the environment. The dominant mechanism can therefore be distinguished by mixing LM foam with the secondary liquid an oxygen-free environment. These experiments confirm that emulsion formation occurs by the addition mechanism. Additionally, a comprehensive analysis of foam-to-emulsion density change, multiscale imaging and surface wettability is presented as a support in Chapter 4.

These results provide an insight into fundamental processes underlying emulsion formation, and they may set a foundation for preparing LM emulsions with a wide range of fluids and controllable properties. Chapter 5 presents some proposed future directions that may be pursued based on this dissertation.

CHAPTER 2

OXIDE MEDIATED MECHANISM OF FOAM FORMATION BY SHEAR MIXING IN AIR

This chapter discusses the mechanism of LM-foam formation and its structure-property-processing relationship. As discussed in the previous section, pure LM has a high density, high surface tension, high reactivity, and rapid oxidation in air. These characteristics limit LM's applicability, make it difficult to spread the LM on to different substrates, and complicate many industrial manufacturing processes. [1] Addition of particles or air bubbles to LM augments its adhesion and rheology which enables deposition and patterning onto many substrates using tools ranging from paintbrushes and stencils to 3D printer nozzles.[39–44] The creation of LM foams through incorporation of air bubbles is particularly compelling because these materials retain fluid or ''paste-like'' characteristics and metallic properties while having a substantially lower metal content (i.e., density and cost).

The prior literature on foaming of high-temperature molten alloys suggests that pre-mixing of solid micro-particles is necessary for foam formation.[45] In contrast, LM foams can be prepared by shear-mixing of LM in air without addition of any solid particles. Resolving this discrepancy, systematic processing–structure–property characterization demonstrates that many crumpled oxide particles are generated prior to air bubble accumulation. The following sections discuss fabrication of LM-foams, onset of foam formation, thermophysical properties of LM foams, and the mechanism of foam formation.

2.1. Fabrication of LM Foams

The LM foams can be fabricated by simple shear-mixing of the pure LM in air. The shear-mixing generates surface waves, some of which fold onto themselves to generate air cavities or air bubbles. The shear-mixing process also generates crumpled gallium oxide flakes, which incorporate into the LM and stabilize air bubbles.

To prepare gallium foam, gallium metal (99.99% from Rotometals) was melted by heating above 30 ℃. 100 g of liquid gallium was taken in a 50 mL beaker and mixed in air at 600 rpm using an industrial mixer outfitted with a 3D printed cross-shaped impeller (Figure 2.1). Figure 2.1a shows that the extended mixing of the LM results in physical transformation of the homogeneous liquid (lustrous cross-section) into a highly heterogeneous foam (diffusely reflecting cross-section).

To gain an insight into the liquid metal foaming process, a high-speed camera (a Photron FastCam mini UX-100) was mounted at a 45 degree angle to image the surface of the LM during mixing. It was revealed that shearing of the LM in both early and later stages generates high amplitude waves and large ripples on the surface of the LM. Some of these waves fold onto themselves, creating cavities that later become air bubbles within the LM (Figure 2.1b). The presence of the air bubbles is evident in the internal structure of the solidified gallium foam (Figure 2.1a).

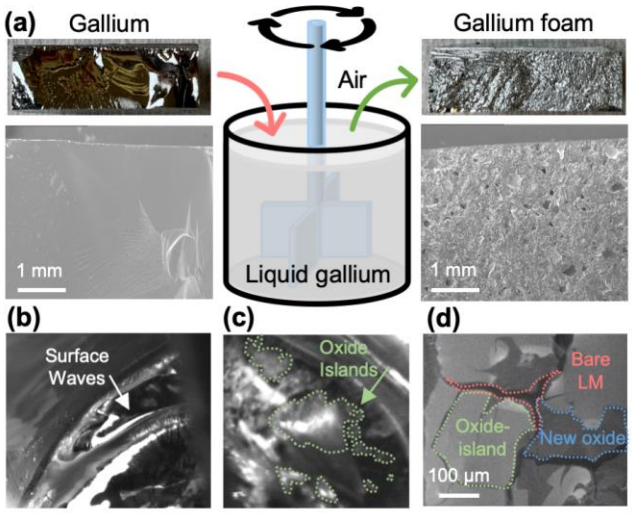

Figure 2.1: (a) Schematic of gallium foam fabrication by shear-mixing of liquid gallium in air; (b) surface waves created by high-speed mixing, (c) gallium-oxide islands on the surface of the stirred LM; (d) focused ion beam image showing oxide-islands generated through ion ablation on the surface of LM in vacuum.

Crumpled gallium oxide flakes are generatred and incorporated by the surface waves created by the shearing-mixing process. A closer inspection of the LM surface during mixing exposes that the surface consists of microscopic ‘‘islands’’ (of gallium-oxide) surrounded by a lustrous ‘‘sea’’ (Figure 2.1c). The diffuse light reflection from the islands reveals that these islands consist of a 1–3 nm thin gallium oxide skin[46] that has wrinkled on nano and micro-scales due to underlying liquid motion.[47] The shear stresses associated with the stirring process fracture the continuous ‘‘old’’ oxide film into floating oxide-islands (as shown in Figure 2.1c). New oxide skin immediately forms on the LM surface exposed to air.

The spontaneous formation of new oxide skin is evident from a previous study where oxide skin from the LM surface was removed in a more controlled fashion by rastering a focused ion beam in a SEM (Figure 2.1d).[48] Even in high vacuum conditions

(10^{-4} Pa), a new, thin oxide begins to form in-between fractured ‘‘old’’ oxide islands within seconds. In atmospheric conditions this process is much quicker, with new oxide emerging in 10^{-5} to 10^{-3} s. [49–51] However, presumably due to the adsorption, dissociation, and surface diffusion of oxygen molecules,[50] the new oxide grows in a non-uniform fractal-like manner. Consequently, much of the surface in-between the ‘‘old’’ oxide micro-islands consist of a very thin and unwrinkled oxide that is highly light-reflecting (or transparent) in nature. Intriguingly, either through macroscopic surface-to-bulk flow near the impeller or through microscopic buckling of the surface waves, many of these islands are internalized as oxide-flakes into the bulk of the LM.

2.2. Onset of Foam Formation

To study the onset of LM foam formation by the shear-mixing process, structural characterization and density measurements of LM foams were performed at different times through-out the mixing process. It was observed that the foam does not start forming until a critical amount of crumpled gallium oxide flakes are internalized. After this point, further shear-mixing results in an increase in air-features in the LM, resulting in reduction in its density over time.

2.2.1. Structural Characterization (Composition of LM Foams)

To evaluate the bulk composition of the mixed LM, a scanning electron microscope (Amray 1910 FESEM employing 20 kV accelerating voltage) was used to image cross-sections of LM samples that were stirred for 0, 2, 3.5, 5, 7.5, 10, 15, 30, 60, 90, and 120 minutes prior to freezing (the samples were simply cleaved with a razor blade). After 2

minutes of mixing, the previously smooth internal surface of the unmixed gallium contains a large concentration of oxide flakes (Figure 2.2). Through internal shearing or prior wrinkling on the LM surface, many of these flakes have crumpled and resemble three-dimensional particles[41,42,44] that can be thought of as microscopic analogs of crumpled paper. The magnified cross-section of one of such particles obtained using cryogenic focused ion beam cross-sectioning[52,53] shows that the crumpled oxide flakes have many, often nanoscale, air voids captured within them (Figure 2.3). As a result, the crumpled flakes are slightly buoyant and are mostly suspended near the top of the sample block.

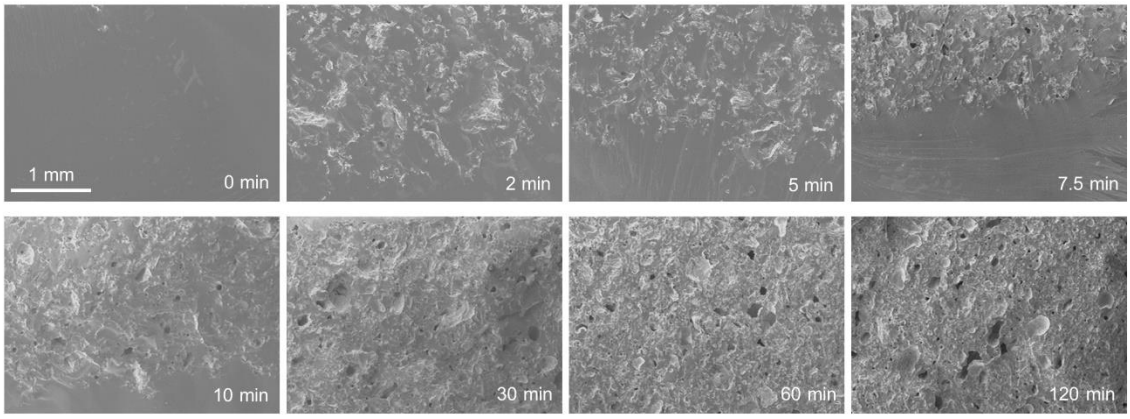

Figure 2.2: SEM images of gallium foam cross-sections processed at different mixing times (0-120 minutes)

Stirring of the LM for another five minutes predominantly leads to accumulation of more of the oxide particles. It is not until 7.5 minutes of mixing that a population of microscopic ($\gg$10 μm) air bubbles can be observed. Since they are surrounded by a thin oxide layer, these air bubbles may be referred as air capsules. LM mixing times between 10 and 30 minutes results in an increased number of the air capsules, which are buoyant and rise to the surface of the sample block. If mixing is continued for longer time (up to

120 minutes), the air capsules and oxide flakes appear to be present in the entire volume of the LM. Naturally, the accumulation of oxide flakes and air capsules significantly alters physical properties especially the density of the foams.

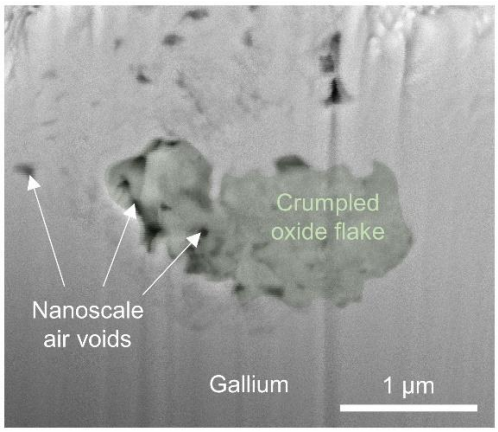

Figure 2.3: SEM image of a crumpled gallium oxide internalized in the bulk LM

2.2.2. Density of LM Foams

The density of each sample of the stirred LM corresponding to different mixing times was measured using the Archimedes principle.[54] Specifically, circular disks of gallium with a 2 cm diameter and a 6 mm thickness were casted using a polymer mold. Then, the buoyant force was measured by suspending the disk in a container of water on an analytical balance.

Despite the evident incorporation of many oxide flakes, the density value for the first 7.5 minutes of stirring remains near the 5.9 g ml^{-1} density of pure gallium (red dotted bar in Figure 2.4). This discrepancy can be resolved by pointing out that the density of the predominant gallium oxide skin phase,[55] β-Ga_2O_3 is also 5.88 g ml^{-1}.[56] Most likely the density value measured is slightly smaller than that of Ga or β-Ga_2O_3 because of the presence of nanoscale air pockets in the crumpled oxide flakes. If stirring is continued for

more than 7.5 minutes, the density of the material begins to decrease substantially, eventually reaching 4.8 gml^{-1} after 2 hours of mixing. Based on the structural characterization, this mixing time threshold (i.e. 7.5 minutes) for density decrease stems from the initiation of air capsule accumulation in the LM.

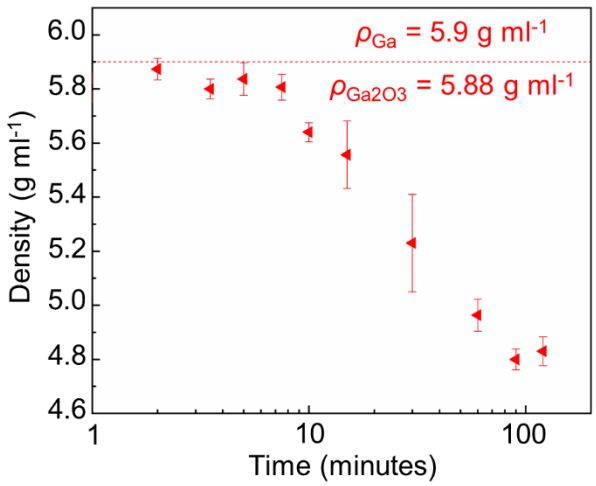

Figure 2.4: Plot of gallium foam density as a function of mixing time

2.3. Thermal and Rheological Properties of LM Foams

To explore the effect of foam formation on important LM properties, measurements were performed for thermal conductivity, viscosity as well as loss and storage moduli of the stirred liquid metal for each of mixing times.

In contrast to the initially unchanged value of density, the plot in Figure 2.5 shows that the thermal conductivity of the LM begins to decrease shortly after the onset of the shear-mixing process. This property was measured using a thermal reference bar method following the modified ASTM D5470 standard.[57,58] Please note that the thermal rather than electrical conductivity was measured because the latter has been previously shown to be only mildly impacted by LM stirring.[41] In contrast, thermal conductivity decreases, even

after just 2 to 5 minutes stirring, from 29 $Wm^{-1}K^{-1}$ (pure gallium) and reaches 18 $Wm^{-1}K^{-1}$ after 2 hours of mixing. The exact mixing time at which the thermal conductivity starts changing is difficult to establish because the initial change is comparable to the experimental uncertainty. In light of the structural characterization, these measurements demonstrate that both the oxide flakes and air capsules significantly disrupt thermal energy carrier transport. Owning to the continuous metal matrix, however, the LM foam thermal conductivity is still much higher than that of elastomer composites with liquid metal inclusions.[58–61]

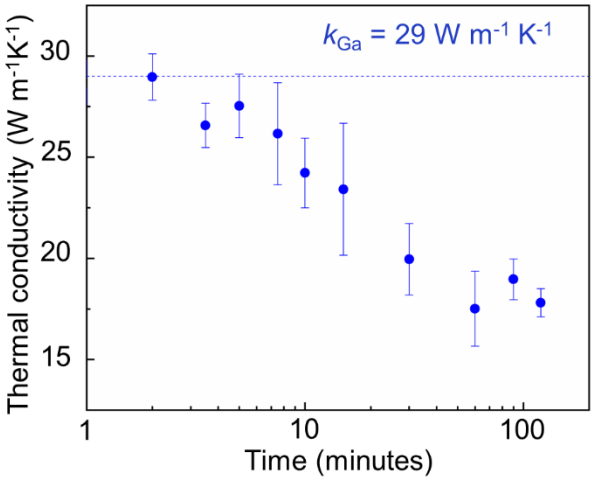

Figure 2.5: Plot of gallium foam thermal conductivity as a function of mixing time

As with the thermal conductivity, the rheological properties of the LM are also significantly impacted through shear mixing. These properties were measured using a TA AR-G2 rotational rheometer equipped with a 40 mm parallel plate geometry and using a gap height of 800 μm. Since the dispersal of oxide flakes throughout the bulk LM phase is analogous to loading of solid particle fillers to the system, it yields an immediate increase

in both viscosity and storage modulus (G'), as seen in the plot in Figure 2.6. A similar trend is observed with the loss modulus (G''), but it was consistently 20–30 times smaller than the storage modulus. The loss modulus is not depicted here as the elastic behavior associated with the storage modulus is of more direct interest. The storage modulus and viscosity reach an initial peak at 7.5 minutes of stirring (1.5 MPa and 1600 Pa s, respectively). The peak at 7.5 minutes corresponds with the point just before many air pockets start being incorporated into the foam. Further mixing results in a rapid drop in the viscosity and modulus, presumably in response to the inclusion air as a ‘‘soft’’ filler. With continued mixing, the modulus and viscosity increase, reaching eventual values of 2.04×10^{-3} and 2193 Pa s, respectively, at a mixing time of 120 minutes. Increased mixing time results in more oxide flakes and air pockets being encapsulated, which has been shown in prior literature to result in an increase in material modulus and viscosity.[62]

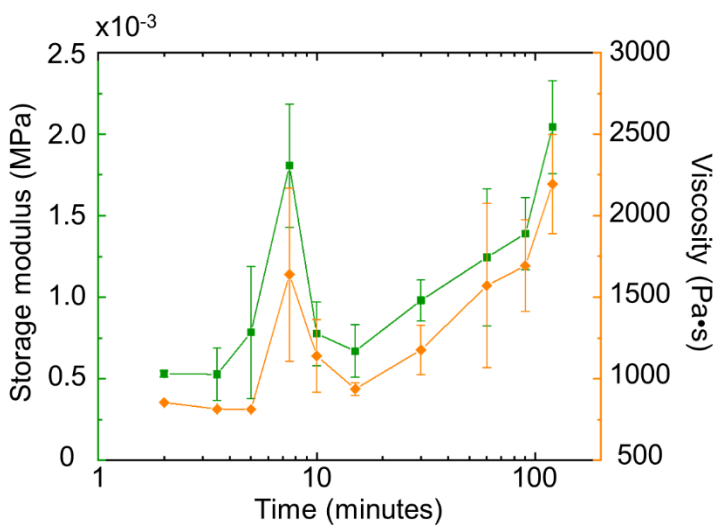

Figure 2.6: Plot of viscosity and storage modulus of gallium foam as a function of mixing time

2.4. Mechanism of Foam Formation

The structural characterization and the plots of thermophysical properties reveal that initially crumpled oxide particles are internalized into the LM. After a critical amount of these particles is reached, they start to stabilize air bubbles within the continuous LM phase. This phenomenon is in one way similar to the foaming of high melting point metals, which require a specific quantity of pre-mixed solid particles for foam stabilization. [63,64] Although a general explanation for the foam stabilizing role of particles has not been agreed on, the structural characterization supports notions of bubble interface stabilization as well as physical bridging of bubbles.[64] Specifically, the representative SEM images in Figure 2.7 show that individual air voids are encapsulated by oxide enclosures. These oxide-enclosures may consist of crumpled oxide particles as well as spontaneously forming oxide shell. Besides, some oxide flakes can extend in-between two such voids bridging the space in between them. The crumpled gallium oxide flakes thus stabilize the LM foam by encapsulating the air voids and by oxide-bridging.

It is important to note that the structure of the LM foams is highly dynamic and most of the geometrical features will change during the mixing. For example, air capsules can coalesce, split or even collapse. This leads to cavities with irregular shapes and a wide range of air capsule sizes. From an application perspective, this random and unpredictable structure may be undesirable because it likely restricts the range of possible properties for the foams.

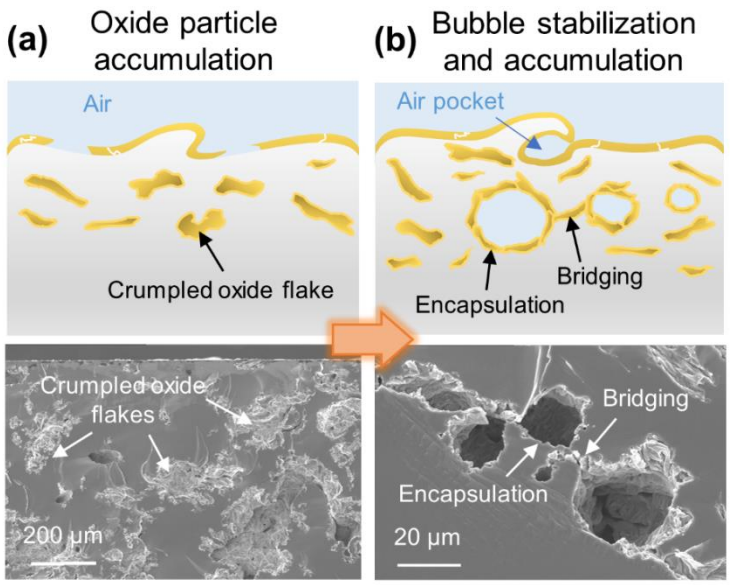

Figure 2.7: Schematic of liquid gallium foaming mechanisms: a) oxide flake accumulation during shear mixing and b) oxide-mediated air capsule stabilization and accumulation.

2.5. Conclusion

The structural and property characterization of shear-mixed liquid gallium shows that like high-melting point metals, near room-temperature LMs require a small volume fraction of solid particles in order to foam. In the case of the LMs, however, the solid particles are not added prior to stirring but are generated during the process by fracturing and internalizing the thin native oxide film at the liquid–air interface. In this setup about 7.5 minutes of mixing is required to accumulate a critical volume fraction of oxide flakes, which crumple into three-dimensional particles that can contain nanoscale air voids, prior to air bubble formation and stabilization. With a different mixing arrangement, this time period might be different. The density, thermal, and rheological properties of gallium foam are highly impacted by the inclusion of oxide flakes and air bubbles. While in general the density and the thermal conductivity decrease, the viscosity and storage modulus first peak

and then continue to increase with the stirring time. These alterations to density and rheology are advantageous for processing, dispensing, and application of the foams. However, the foaming of LMs does not stop its corrosion and embrittlement of other metals, which may cause physical damage to metallic substrates upon contact. Next section addresses this challenge by investigating incorporation of a secondary liquid that impede's LM's reactivity.

CHAPTER 3

GALLIUM-OXIDE STABILIZED OIL-IN-LIQUID METAL EMULSIONS

This chapter discusses the incorporation of a secondary liquid (silicone oil) into the LM-foam resulting in "oil-in-LM" emulsion formation. This emulsion, in addition to having better process-ability and considerable thermal conductivity, prevents corrosion and embrittlement of other metals. This makes them particularly suitable for applications in thermal interface materials (TIMs).

While dispersing LM into another fluid medium is relatively simple, the opposite is more challenging owing to LM's high density and surface tension as well as immiscibility with other liquids.[65] When one immiscible liquid more favorably emulsifies into another liquid, such as LM into silicone oil, inverting this emulsion orientation typically requires the introduction of emulsifying agents or surfactants.[66,67] This section demonstrates that stable ''oil-in-LM'' emulsions can be created through the incorporation of silicone oil (SO) into LM-based foam.

The following sub-sections discuss the method of fabrication of LM-emulsions, impact of secondary liquid's viscosity on the emulsion structure and its phase inversion characteristics. Additionally, the impact of volumetric content of the secondary liquid (SO) on the structure and properties of the oil-in-LM emulsion are discussed.

3.1. Fabrication of LM Emulsions

LM Emulsions can be fabricated by simple shear mixing of LM with a secondary liquid in air without any specialized processing techniques. These emulsions can be divided into two broad categories, LM-in-liquid and liquid-in-LM emulsions, depending of which fluid takes the disperse or the continuous phase. When silicone oil (SO) is used as a

secondary liquid, mixing it with the 'pure LM' results in fabrication of LM-in-oil emulsion. Whereas the oil-in-LM emulsions can be created through the incorporation of silicone oil (SO) into LM-based foam (as shown in Figure 3.1a). Figure 3.1b shows that previously air-pockets in LM-foam are replaced by SO-droplets in the Oil-in-LM emulsion.

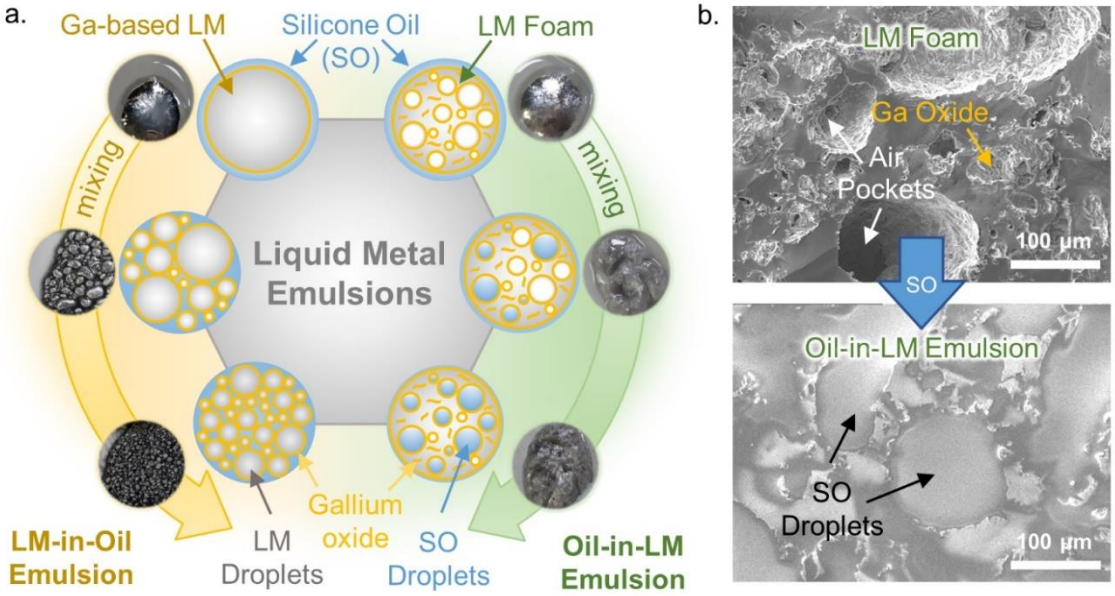

Figure 3.1: (a) Overview of shear-mixing based fabrication of LM-in-oil emulsions and oil-in-LM emulsions and (b) cross-sectional SEM images of LM-based foam before and after mixing with silicone oil (SO) which results in the formation of oil-in-LM emulsion.

For fabrication of these emulsions, Gallium (99.99%) was purchased from Rotometals while the silicone oils with viscosity ranging from 10 to 10 000 cSt were obtained from Sigma Aldrich. The LM-in-oil emulsions were prepared by manually mixing the pure and melted gallium with the silicone oil in specific volume ratios for various periods of time in a small plastic container using a wooden stir rod. In all cases, this procedure resulted in formation of LM droplets within the oil phase. The oil-in-LM

emulsions were prepared in a two-step process: first the stirring of LM in air to create LM foam, followed by mixing of LM foam with oil. In the first step, LM foam was fabricated by shear-mixing the liquid gallium in air (as described in Chapter 2). In the second step, LM foam and silicone oil in specific volume ratios were mixed manually in a small plastic container using a 2.1 mm thick wooden stirring rod. To keep the liquid metal in molten state during all mixing processes, the container was kept on top of a hot plate set at 60 ℃.

3.2. Effect of Viscosity and Mixing Time on Emulsion Formation

The visocity of silicone oil and the mixing duration significantly affect the structure and properties of both types of LM based emulsions. In the case of LM-in-Oil emulsions, the mixing of melted gallium with SO leads to formation of the LM droplets whose size depends on the viscosity of the oil as well as the mixing rate and time. Figure 3.2a shows images of LM-in-oil emulsions formed by 30 minutes of manually mixing 10, 100, 1000, and 10 000 cSt SOs into LM at a 20:80 volume ratio. In the 10 cSt SO, the LM separates into a widely distributed mix of large droplet sizes (greater than 1 mm) and smaller sizes. Since the shear stress that leads to droplet breakup scales with the viscosity, the average LM droplet size distribution becomes smaller for higher viscosity oils.[68,69] For example, within 30 minutes of mixing in the 10 000 cSt SO, the droplet size is reduced to tens of microns or smaller. While the oil viscosity does not impact the effective thermal conductivity of the LM-in-oil emulsions under mild compression (~2 mm thick samples under 0.1 MPa pressure have values under 2 W m^{-1} K^{-1} that match the prior results for silicone pads with LM droplets[60,70]), it does have a strong influence on the dynamics of formation of emulsions with inverted phases.

The generation and incorporation of oxide flakes and oxide-covered air bubbles into LM is necessary to form oil-in-LM emulsions. Prior to addition of the SO, the LM foam was generated through 2 hours of rapid shear mixing of melted gallium at 600 rpm in an air environment.[71] This material contains a mixture of wrinkled gallium oxide flakes, oxide-covered air bubbles, and occasional air pores with sizes ranging from a tenth to hundreds of micrometers (as shown in Figure 3.1b). With these internal features, SO readily mixes into the foam (at 20:80 SO:LM-foam volume ratio) within several minutes of manual shear mixing of the two liquids at about 120 rpm. The cross-sectional electron micrographs in Figure 3.1b and optical images in Figure 3.2b clearly show that much of the SO disperses into distinct droplets surrounded by the continuous LM phase with the foam features (as shown through the glossy reflections on the cross sectioned surfaces). Since the SO contains dissolved air, the oil droplets are likely covered by a gallium oxide shell. Using this approach, oil-in-LM emulsions can be created with silicones with viscosity ranging from 10 to 10 000 cSt.

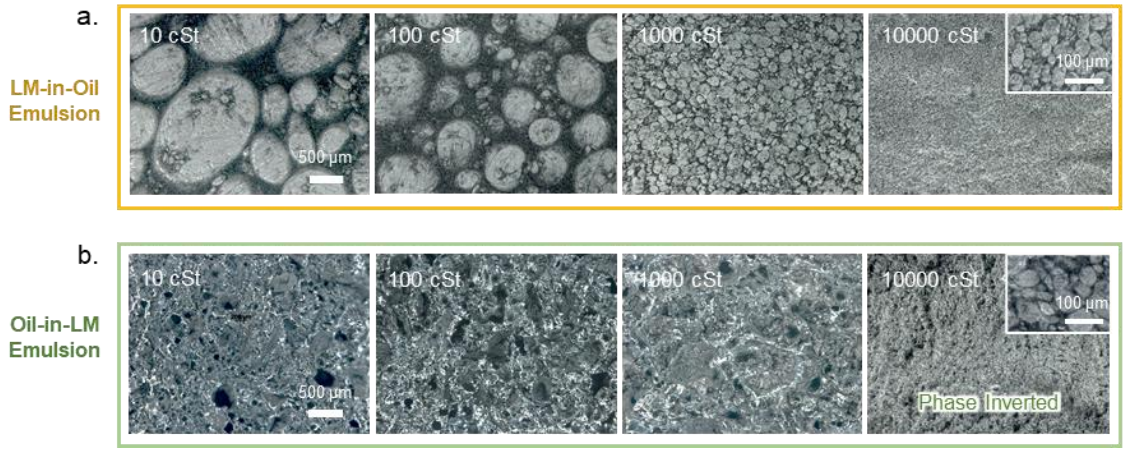

Figure 3.2: (a) optical images of LM-in-oil emulsions made with 10 to 10,000 cSt viscosity SOs (20:80 SO:LM volume ratio and 30 minutes of mixing), (b) optical images of oil-in-LM emulsion cross sections made with 10 to 10,000 cSt viscosity SOs (20:80 SO:LM foam volume ratio and 30 minutes of mixing)

3.3. Phase Inversion of Oil-in-LM Emulsion upon Extensive Mixing

Extended stirring of the oil-in-LM emulsions produces vastly different outcomes that depend on the used oil viscosity. Specifically, the schematic and images in Figure 3.3a show that continued mixing of the oil-in-LM emulsion containing the 10 000 cSt SO results in gradual break-up of the emulsion into smaller regions separated by oil and eventual phase inversion into an LM-in-oil emulsion. The illustrative processing map in Figure 3.3b shows that for the specific case of 20:80 SO:LM foam volume ratio, the decrease in oil viscosity delays or significantly inhibits the onset of this inversion. For example, no inversion of the phases was observed when using the 10 cSt even after 120 minutes of stirring. It is important to note that this illustrative processing map is meant to reflect the different phase stability regions and can change based on changes in processing conditions. In addition, the transitions between the phases are gradual, so the boundaries on the processing map are blurred. Next section investigates how the volumetric content of the SO in these inversion-resistant (‘‘stable’’) oil-in-LM emulsions impacts their internal structure.

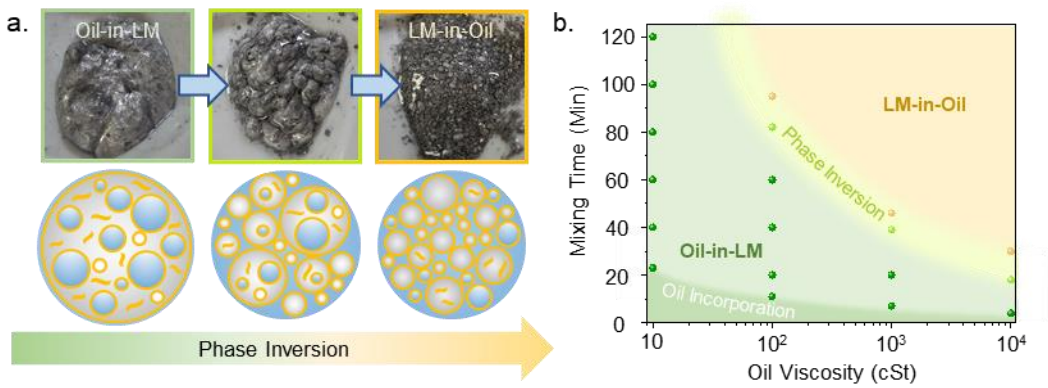

Figure 3.3: (a) illustrative images and schematics showing phase inversion of oil-in-LM back into LM-in-oil emulsions upon excessive mixing, and (b) illustrative processing map showing the oil-in-LM formation window and phase inversion regions (20:80 SO:LM foam volumetric ratio, 120 rpm manual shear mixing).

3.4. Effect of Volumetric Content of SO on Oil-in-LM Emulsion

The volumetric content of SO significantly affect the structure and properties of the oil-in-LM emulisons. Figure 3.4a shows electron micrographs of oil-in-LM emulsions created by 30 minutes of mixing of LM foam with different volume fractions of 10 cSt SO. The duration for full internalization of the oil into the foam increased from under 5 minutes to about 30 minutes with increase of the SO:LM foam volumetric ratio from 10:90 to 40:60 (higher ratios are not used in the studies because excess oil outside the emulsion was observed even for longer mixing times). Within the studied range, the increase in the SO mixing content results in a corresponding increase in SO pockets observed in the sample cross sections (as shown in Figure 3.4a). In addition to formation of these closed-cell features, the SO also appears to fill many of the open-cell pores that are produced during the chaotic LM foam fabrication. This dynamic multiscale structure of the starting LM foams also makes it infeasible to provide a more quantitative description of the impact of the oil content and viscosity on the oil-in-LM emulsion structure. However, the large

differences in the thermal conductivity of the various emulsions (describe next) implies that such differences in the internal structure could be substantial.

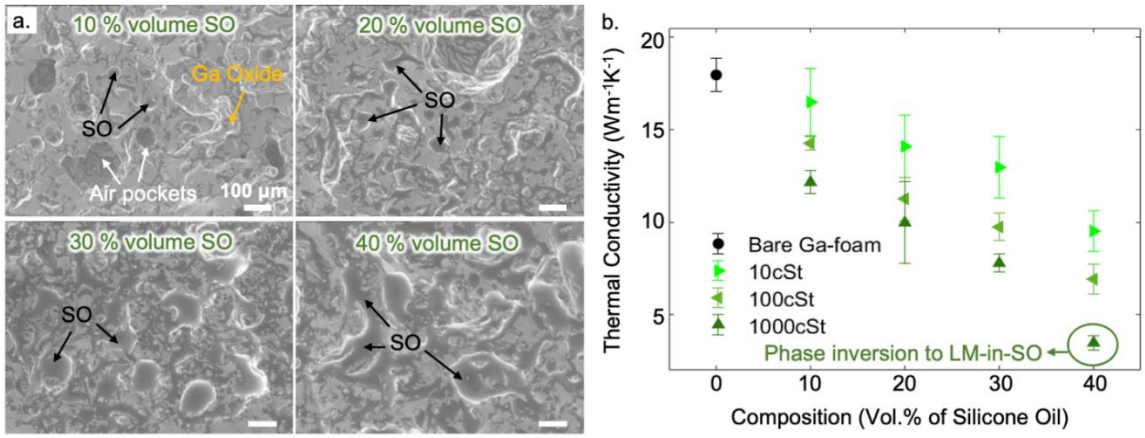

Figure 3.4: (a) SEM micrographs of oil-in-LM emulsions cross-sections made with 10 cSt viscosity SO with SO:LM foam volumetric ratio ranging from 10:90 to 40:60, (b) plot of the effective thermal conductivity against the SO volume percentage for oil-in-LM emulsions.

The effective thermal conductivity (k_{eff}) of oil-in-LM emulsions decreases with both the increase in the oil content and its viscosity (as shown in Fig. 19b). Due to its relevance to thermal interface materials (TIMs) application, these measurements were conducted by a steady-state stepped bar apparatus following the modified ASTM D5470 standard. This measurement methodology reflects the impact of both the intrinsic material property and sample-measurement bar contact resistances (i.e., provides the effective thermal conductivity of the sample).[57,72] For LM-based samples, the effect of the thermal contact resistance is small, so the effective values reported here are close to the intrinsic material value.[73] For example, the pure melted gallium measured 28.7 $\pm$ 1.1 $Wm^{-1}K^{-1}$ that agrees with prior literature value.[74] Incorporation of the oxide flakes, air bubbles, and pores during 120 minutes of stirring the melted gallium at 600 rpm decreases the k_{eff} of the

gallium foam to 17.8 $\pm$ 0.7 $Wm^{-1}K^{-1}$ (this value is not impacted by an additional 30 minutes of low speed manual mixing at 120 rpm).

When the SO is incorporated into the foam within 30 minutes of mixing, the k_{eff} of the oil-in-LM emulsions experiences a decrease proportional to the increasing oil volume content (by about 10 W m^{-1} K^{-1} in the worst case of 40:60 100 cSt SO:LM foam). This result is counterintuitive as the replacement of the low thermal conductivity air (k = 0.024 W m^{-1} K^{-1}) content with the more conductive SO (k = 0.2 to 0.3$Wm^{-1}K^{-1}$) should increase the emulsion's thermal conductivity. Since the k_{eff} of the LM-foam is not impacted by the additional 30 minutes of mixing without the oil (and the generated oxide and air features), the SO likely does not replace most of the air features (e.g., fill closed air bubbles) but creates additional oil-filled structures. Compared to pure LM or even LM foam, the oil-in-LM emulsions show reductions in effective thermal conductivity. Thus, the addition of these oil-filled structures in combination with air bubble and gallium oxide content appears to disrupt the thermal energy carrier transport through the composite. The increasing oil viscosity likely alters the quantity and size of such features, thereby resulting in a greater decrease of the emulsion's k_{eff}. Despite this decrease, the 9.5 $\pm$ 1.1 $Wm^{-1}K^{-1}$ k_{eff} of the SO:LM 40 : 60 with 10 cSt SO is still multiple times higher than that of typical silicone grease TIMs measured in the same way (1 to 4 $Wm^{-1}K^{-1}$). Next section demonstrates that the presence of the oil provides additional anti-corrosive characteristics to the emulsions that make them uniquely suitable for TIMs.

3.5. Preventing Corrosion of Aluminum Substrates

Generally, the LM embrittlement of aluminum is rapid and takes place within hours of direct contact with the gallium. With sufficient content of the SO, the oil-in-LM

emulsions do not embrittle aluminum. This characteristic of the LM foams and emulsions was tested by placing the samples in between two aluminum sheets and applying 0.1 MPa of pressure. The experimental setup was heated to 60℃ to ensure the sample was in the liquid state. The representative images and bar plot in Figure 3.5a and b show that after 24 hours the LM foams corroded the aluminum foil in all the 20 experimental repetitions. The chance of preventing aluminum embrittlement is dramatically improved with addition of even a small amount of the SO (e.g., by 50% for the 10:90 SO:LM foam composition) and increases nearly linearly with further oil addition. Furthermore, the emulsions with the 40:60 SO:LM foam composition did not corrode aluminum foil in any of the 20 experimental repetitions lasting 24 hours (each exposing the samples to aluminum foil on two sides) or in extended 7 day trials.

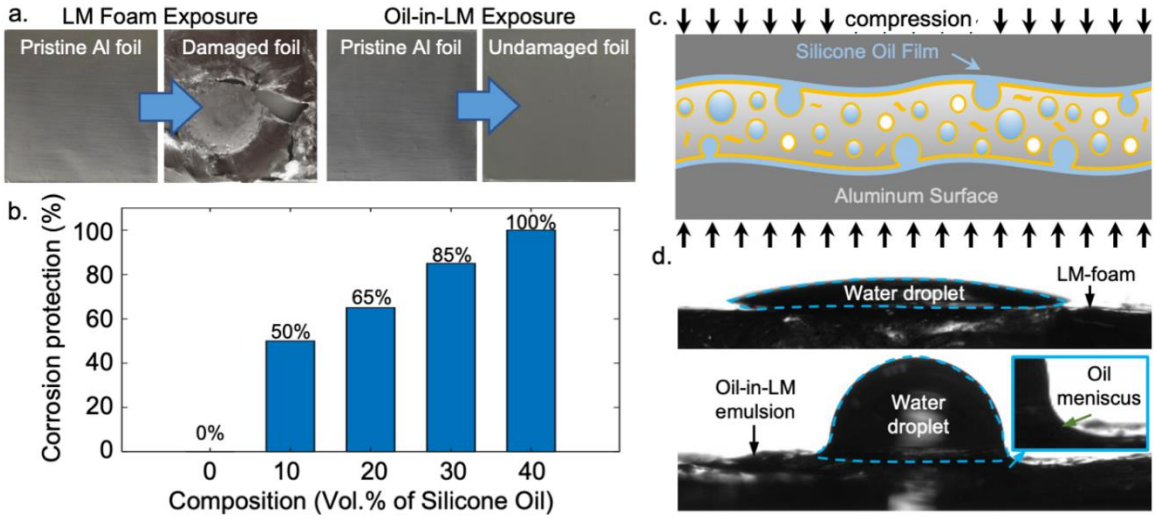

Figure 3.5: Corrosion protection characteristics of oil-in-LM emulsions (a) representative images of aluminum foil before and after 24-hour contact under 0.1 MPa pressure with LM foam and oil-in-LM emulsion (40:60 SO:LM foam), (b) bar plot showing corrosion protection ability of 10 cSt oil-in-LM emulsions made with varying oil content (total 20 tests were performed for each composition), (c) schematic illustrating the mechanism of aluminum corrosion protection under compression: wetting of the exterior of the emulsions by a thin film of SO, and (d) images of 1 microliter water droplets placed on LM foam and on the 40:60 oil-in-LM emulsion.

The corrosion inhibiting characteristic of the LM-in-oil emulsions likely stems from the presence of a thin SO film on the exterior of the material that provides a barrier between the gallium and aluminum (as shown in Figure 3.5c). The presence of this exterior SO film was confirmed by placing small water droplets on the LM foam and on the emulsion with 40:60 SO:LM foam composition. The images in Figure 3.5d show that the water droplet contact angle increases from about 10° on the LM foam to about 90° on the oil-in-LM emulsion. Since the latter value is in the range of water contact angles typically measured for SO impregnated textured or porous surfaces,[75–77] the exterior surface is likely entirely covered by an oil film. Furthermore, the presence of the oil meniscus around the perimeter of the water droplet sitting on the oil-in-LM emulsion provides additional evidence of the surface oil film.[78] The oil likely wets the exterior oxide created during the mixing process as well as any new oxide that might be created while applying the emulsion onto the aluminum foil. With about 40% of the emulsion volume occupied by oil, there is an ample supply of it to cover the entire surface prior to contact with a substrate or even during potential volume disruption when making contact (i.e., oil can wick out of pores or leak from ruptured ‘‘bubbles’’ under compression). This characteristic of corrosion prevention together with a good thermal conductivity, make this emulsion a promising candidate for TIM application.

3.6. Conclusion

This section demonstrated that foam features in LM (oxide flakes, air bubbles, and pores) enable internalization of a secondary liquid, resulting in formation of stable “oil-in-LM” emulsions. Although these emulsions can be created using oils with viscosity ranging

from 10 to 10,000 cSt, it was revealed that beyond a proper viscosity and mixing time "processing window," the created materials can invert into the more common LM-in-oil emulsions. In particular, the oil-in-LM emulsions made with lower viscosity (10 cSt) silicones proved to be resistant to phase inversion up to the tested 120-minute mixing time. The use of lower viscosity oils is also beneficial from thermal perspective as it leads to the lowest decrease in the effective thermal conductivity of the emulsions. The corrosion prevention of these emulsions increases with the volumetric content of 10 cSt silicone oil (SO). Eventually, the 40:60 SO:LM foam emulsions have sufficient 10 cSt SO to entirely prevent the possibility of gallium-induced corrosion of the metal substrate. At this composition, this stable oil-in-LM emulsion has an effective thermal conductivity of 9.5 ± 1.1 $Wm^{-1}K^{-1}$ that is several times higher than currently available TIM greases or pads. Besides TIM application, the insights gathered from these processing-structure-property relationships of oil-in-LM emulsions may benefit further exploration and the use of these new liquid phase composites in other soft applications.

Prior to this study, it was expected that replacing the non-conductive air pockets in LM-foam with relatively conductive SO would improve the thermal transport. Contrarily, the addition of SO disrupts the thermal transport, likely due to oil creating microscale features in addition to the existing foam features (*i.e.*, the oil does not appear to completely displace air in the existing features). This discrepancy arises due to little understanding of the mechanism of emulsion formation. Particularly, whether the secondary liquid internalizes by displacing air from existing foam features or by creating additional microscale features. Addressing this question is important for further research on improving material properties and controlled fabrication of these emulsions. The following

chapter aims to address this question by a systematic investigation of the mechanism of emulsion formation, leading to completion of this dissertation research.

CHAPTER 4

EMULSION FORMATION MECHANISM

In the previous chapters, it was discussed that shear mixing the bulk LM in air results in LM-air-foam formation. This LM-foam is stabilized by oxide flakes, oxide enclosures, and oxide feature-bridging in-between capsules. The LM-foam in turn enables internalization of secondary liquid resulting in liquid-in-LM emulsion formation. Like LM foam, the emulsion must be stabilized by oxide flakes and oxide enclosures. However, unlike LM foam, the liquid-in-LM emulsion is stable only within a limited property-processing window, beyond which it inverts to the more common LM-in-liquid emulsion. This section systematically investigates the fundamental processes underlying the formation of these liquid-in-LM emulsion.

The incorporation of a secondary liquid into the LM foam can occur by two possible microscale mechanisms (i.e. replacement and addition mechanism). The first mechanism consists of the secondary liquid filling the existing air pockets in the LM foam (thereby replacing air), whereas the second mechanism consists of secondary liquid creating additional features within the LM foam. The following sections discuss these two mechanisms and methods for identifying the underlying mechanism for liquid-in-LM emulsion formation. Specifically, it has been elucidated that the two mechanisms cause opposing changes in density for conversion of LM foam to emulsion. Furthermore, change of environment from air to nitrogen can affect the emulsion formation and provide key information about the formation mechanism. This is followed by comprehensive analysis of density, surface wettability and multiscale imaging. Finally, the thermal properties and

prevention of aluminum embrittlement of these materials are discussed from the perspective of thermal management applications.

4.1. Two Mechanisms of Liquid-in-LM Emulsions Formation

4.1.1. Description

In principle, liquid-in-LM emulsions can be formed through the incorporation of the secondary liquid into the LM foam via the two routes illustrated in Figure 4.1. First, the secondary liquid could replace the air inside existing features within the foam (as shown in Figure 4.1a). In this "replacement mechanism", the secondary liquid fills open-cell features such as pores (as shown in Figure 4.1b**)**, but also could replace air within capsules ruptured at the foam-secondary liquid interface during mixing (as shown in Figure 4.1c). Second, additional gallium oxide-enclosed secondary liquid closed-cell features ("capsules") can form during the perturbation of the oxide at the two bulk fluid interfaces throughout the mixing process (as shown in Figure 4.1d-e). This "addition mechanism" of secondary liquid requires the continual formation of oxide at the two bulk fluids interface. Some oxide regrowth could also be needed to seal ruptured capsules in which secondary liquid replaced the air. As for foams, the mechanical stabilization of the emulsions requires the presence of oxide fragments or potentially other solid particles within the LM that prevent the buoyancy-driven escape of secondary liquid by bridging the space between capsules.

Next section presents theoretical derivations for the expected density of the emulsions and show that the predominant mechanism by which secondary liquid

incorporates into the LM foam can be distinguished from the foam-to-emulsion density change.

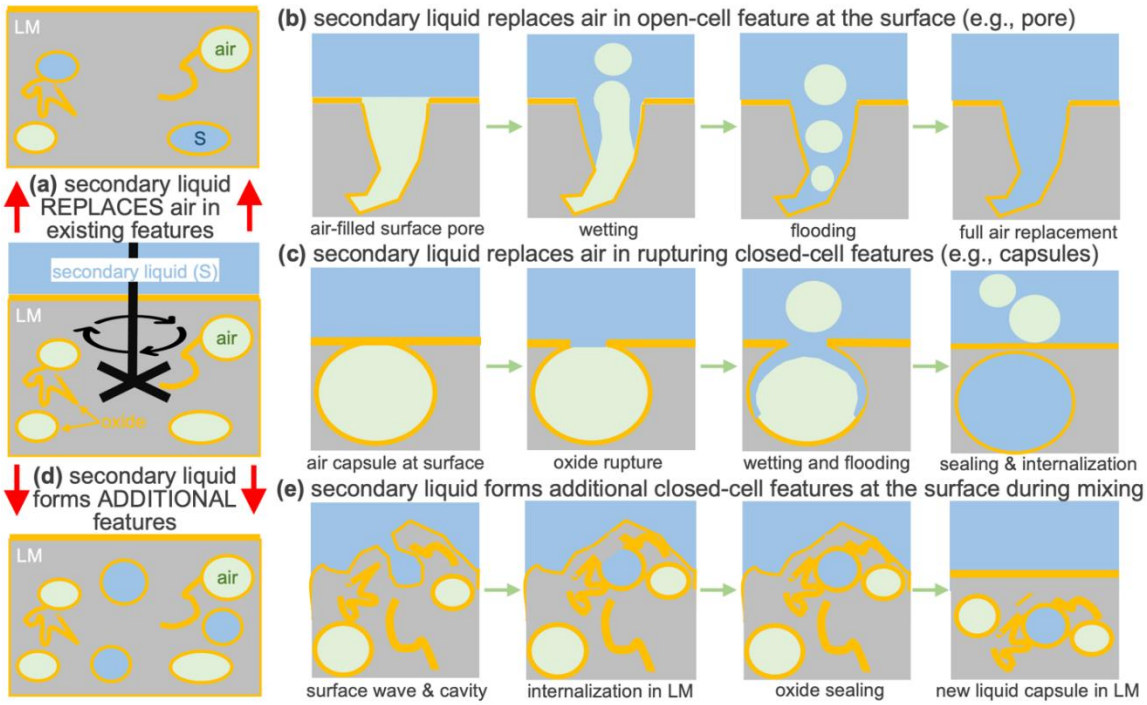

Figure 4.1: Schematics of possible emulsion formation mechanisms: (a) air replacement by the secondary liquid (S), exemplified as (b) air-replacement in open-cell and (c) closed-cell geometrical features; (d) secondary liquid forming additional closed-cell geometrical features in LM foam, exemplified as (e) formation of liquid-filled cavities by surface wave cresting.

4.1.2. Theoretical LM Foam-to-Emulsion Density Difference

The density of the LM foam, ρ_f, can be expressed with volumes and densities of its components as:

$$\rho_f = \frac{V_a\rho_a + V_{LM}\rho_{LM} + V_{ox}\rho_{ox}}{V_a + V_{LM} + V_{ox}} \tag{1}$$

where V is the volume and ρ the density of the air (subscript a), liquid metal (subscript LM), and oxide (subscript ox) components. For the specific case in this work, the density

of the LM oxide and the LM are nearly identical ($\rho_{LM} \approx \rho_{ox} \approx 6$ g cm^{-3}),[71] Eq.1 can rewritten as:

$$\rho_f = \frac{V_a\rho_a + (V_{LM}+V_{ox})\rho_{LM}}{V_a + V_{LM} + V_{ox}} \tag{2}$$

In addition, the oxide is only present in ~1 to 3 nm thick films,[28,46] so the volume it occupies is much smaller than that of the LM or air (i.e., $V_{ox} \ll V_{LM}$ and $V_{ox} \ll V_a$). Accordingly, the analysis can be simplified by assuming that the oxide volume is negligible:

$$\rho_f \approx \frac{V_a\rho_a + V_{LM}\rho_{LM}}{V_a + V_{LM}} \tag{3}$$

If the secondary liquid with density ρ_s is incorporated into the LM foam purely through the air replacement mechanism (Figure 4.1a-c), there should be either no change or a very minor change in the total volume during the process. In other words, it can be assumed that the secondary liquid volume (V_s) replaces some fraction of the air volume present in the foam (V_a), which leads to a reduced air volume (V_a^*) within the emulsion ($V_a^* = V_a - V_s$). As such, the density of the emulsion formed with the air replacement mechanisms is (ρ_{e-r}):

$$\rho_{e-r} = \frac{V_a^*\rho_a + V_{LM}\rho_{LM} + V_s\rho_s}{V_a^* + V_{LM} + V_s} = \frac{(V_a - V_s)\rho_a + V_{LM}\rho_{LM} + V_s\rho_s}{V_a - V_s + V_{LM} + V_s} = \frac{V_a\rho_a + V_{LM}\rho_{LM} + V_s(\rho_s - \rho_a)}{V_a + V_{LM}} \tag{4}$$

Combining Eq. 3 and Eq.4, we obtain:

$$\rho_{e-r} = \frac{V_a\rho_a + V_{LM}\rho_{LM}}{V_a + V_{LM}} + \frac{V_s(\rho_s - \rho_a)}{V_a + V_{LM}} = \rho_f + \frac{V_s(\rho_s - \rho_a)}{V_a + V_{LM}} = \rho_f + \phi_s^*(\rho_s - \rho_a) \tag{5}$$

where $\phi_s^* = V_s/(V_a + V_{LM}) = V_s/(V_a^* + V_{LM} + V_s)$ is the volume fraction of the secondary liquid in the emulsion formed through the replacement mechanism.

On the other hand, if the secondary liquid (assumed to be incompressible) is incorporated into the LM foam purely through the addition mechanism, the total volume of the resulting emulsion will be higher than that of the input foam by a factor of $\lambda = (V_a + V_{LM} + V_s)/(V_a + V_{LM})$. This factor can be expressed in terms of the volume fraction of secondary liquid in the addition mechanism (ϕ_s) as $\lambda^{-1} = (V_a + V_{LM})/(V_a + V_{LM} + V_s) = 1 - V_s/(V_a + V_{LM} + V_s) = 1 - \phi_s$. As such, the density of the emulsion formed with the secondary liquid addition mechanisms (ρ_{e-a}) is:

$$\rho_{e-a} = \frac{V_a\rho_a + V_{LM}\rho_{LM} + V_s\rho_s}{V_a + V_{LM} + V_s} = \frac{V_a\rho_a + V_{LM}\rho_{LM} + V_s\rho_s}{\lambda(V_a + V_{LM})} = \lambda^{-1}\frac{V_a\rho_a + V_{LM}\rho_{LM} + V_s\rho_s}{V_a + V_{LM}} \quad (6)$$

Combining Eq. 3 and Eq.6, we obtain:

$$\rho_{e-a} = \lambda^{-1}\left[\frac{V_a\rho_a + V_{LM}\rho_{LM}}{V_a + V_{LM}} + \frac{V_s\rho_s}{V_a + V_{LM}}\right] = \lambda^{-1}\left[\rho_f + \rho_s\frac{\{V_s + V_a + V_{LM} - (V_a + V_{LM})\}}{V_a + V_{LM}}\right] \quad (7)$$

Through algebraic manipulation and substitution of the definition of λ, Eq.7 can be simplified as:

$$\rho_{e-a} = \lambda^{-1}\left[\rho_f + (\lambda - 1)\rho_s\right] = (1 - \phi_s)\rho_f + \phi_s\rho_s = \rho_f - \phi_s\left(\rho_f - \rho_s\right) \quad (8)$$

The derived Eq.5 and Eq.8 demonstrate that the two secondary liquid incorporation mechanisms have an opposing impact on the foam-to-emulsion density change. Specifically, since any secondary liquid is denser than air ($\rho_s > \rho_a$), emulsions formed under the air replacement mechanism will always be denser than the original foam (*i.e.*, $\rho_{e-r} > \rho_f$ for $\phi_s > 0$). In contrast, when the LM foam is denser than the secondary liquid ($\rho_s < \rho_f$ as for silicone oil and our foams), emulsions formed through the addition mechanism will be lighter than the original foam (*i.e.*, $\rho_f > \rho_{e-a}$ for $\phi_s > 0$). Furthermore, both the positive and negative density difference ($\rho_{e-r} - \rho_f$ or $\rho_{e-a} - \rho_f$) should be proportional to the volume fraction of incorporated secondary liquid in the emulsion. Next

section experimentally explores the two fluid mixing processes and compares the results against the analytical predictions.

4.2. Identifying Underlying Mechanism for Formation of Liquid-in-LM Emulsion

4.2.1. Analysis of Density of Silicone Oil and LM Foam Mixed in Air and Nitrogen Environments

To investigate emulsion formation mechanism, silicone oil (10 cSt) and eGaIn foam were manually mixed for 30 minutes in either air[30] or nitrogen environments (as shown in Fig. 4.2a-b). As expected, mixing within an air environment leads to the incorporation of all the oil into the LM foam and formation of a stable silicone oil-in-LM emulsion (as shown in Figure 4.2a).[30] In contrast, no silicone oil mixing into the LM foam is observed visually in a nitrogen environment (as shown in Figure 4.2b). In more quantitative terms, the measurements in Figure 4.2c show that the density of the LM foam after mixing with any volume fraction of silicone oil in a nitrogen environment is only 0.1 to 0.3 g cm^{-3} (2 to 6%) higher than that of the original foam. Similarly, the density of the LM emulsion (*i.e.*, silicone oil and LM foam mixed in an air environment) with only a 10% oil input volume fraction is about the same as that of the original foam. However, with more silicone oil added, the density of the emulsion decreases linearly with the secondary liquid's input fraction. For the 40:60 input volume ratio between the silicone oil and LM foam, the emulsion density is ~1 g cm^{-3} (20%) lower than the original foam.

The linear decrease of the emulsion density with increasing input oil volume fraction past the 10% threshold agrees with Eq.8 predictions. This observation provides support for the occurrence of the secondary liquid addition emulsion formation mechanism

(Figure 4.1d-e). In the case of the fluid mixing in nitrogen, the lack of oxygen in the environment likely prevents the continual growth of an oxide shell that is critical to the stability of the new silicone oil capsules.

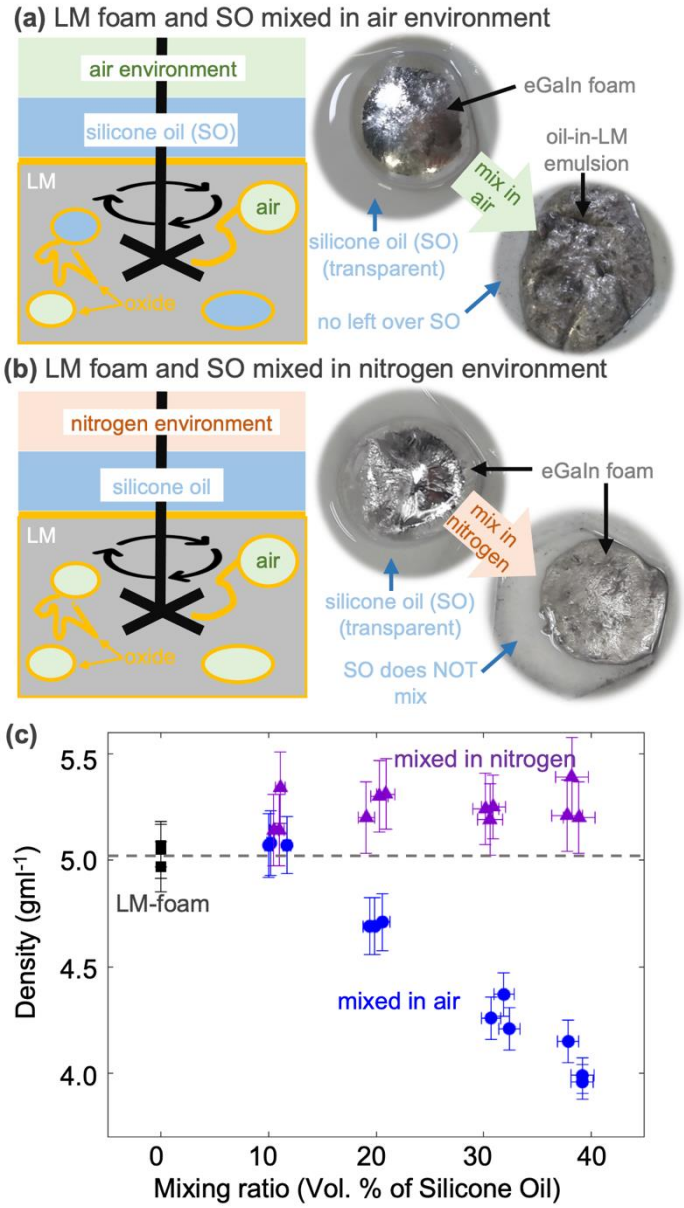

Figure 4.2: Schematics and example images of LM foam and silicone oil (SO) mixing in (a) an air (i.e., the emulsion) and (b) nitrogen environment; (c) the density of the LM materials resulting from the two mixing processes with varying input volumetric ratios of SO and LM foam.

To provide further evidence that the lack of oxide growth prevents stable silicone oil capsule formation, an “oxide forming” liquid (hydrogen peroxide)[79] was mixed with the LM foams in both environments. In other words, this decouples the oxide-shell formation from the mixing environment oxygen content. Confirming that oxide growth is necessary for the silicone oil capsule stability, the hydrogen peroxide was incorporated into the LM foam in both environments (as shown in Figure 4.3).

Oxide growth prevention could also inhibit the silicone oil from replacing air in rupturing capsules because they could not be re-sealed (as shown in Figure 4.1d). However, the data trend agreement between the density measurements and Eq. 8 indicates that the air replacement mechanism does not occur for geometrical features within the bulk of the foam. This observation allows to propose an explanation for the minor density increase when mixing oil and the LM foam in nitrogen and when mixing small (i.e., 10%) silicone oil volume fractions with the LM foam in air. Specifically, in both cases, the silicone oil likely replaces air within “open-cell” features on the foam surface. Since these open-cell features are only present on the surface, they are limited in number, and their filling leads to a much smaller density change than the addition of the much more abundant oil capsules. In the following sections, further evidence is provided for this explanation of the density measurements using surface wettability measurements and multiscale imaging.

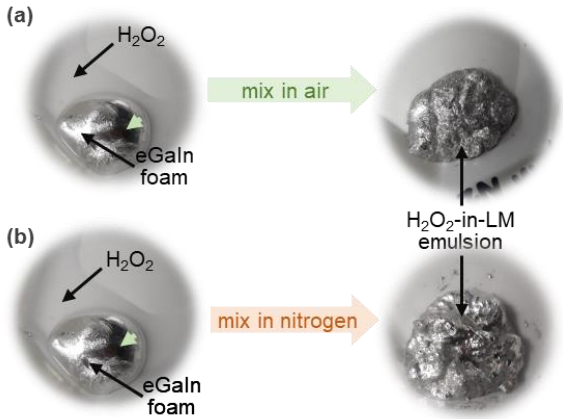

Figure 4.3: Mixing of LM foam with hydrogen peroxide in (a) air and in a (b) nitrogen environment

4.2.2. Surface Wettability and Multiscale Imaging of the Silicone Oil Mixed with the LM Foam in Air and Nitrogen Environments

The presence of silicone oil on the surface of the LM foam or emulsion strongly impacts the surface water contact angle. In particular, the plot in Figure 4.4 shows that while the LM foams are hydrophilic with contact angles varying from about 10º to 40º, the emulsions are nearly or slightly hydrophobic with contact angles of about 80º to 95º. The substantial increase of the water contact angle with the silicone oil addition implies that the oil forms a continuous surface. The resulting hybrid solid-liquid surface is analogous to oil-impregnated surfaces.[80,81] In contrast, the water droplets placed on the surface of the LM foam mixed with silicone oil in the nitrogen environment have contact angles varying greatly between 35º to 90º. This observation implies that mixing the foam and silicone oil in the nitrogen environments leads to only partial coverage of the LM foam surface by the silicone oil. Next, the surface and cross-sectional morphology of these materials is explored using multiscale imaging.

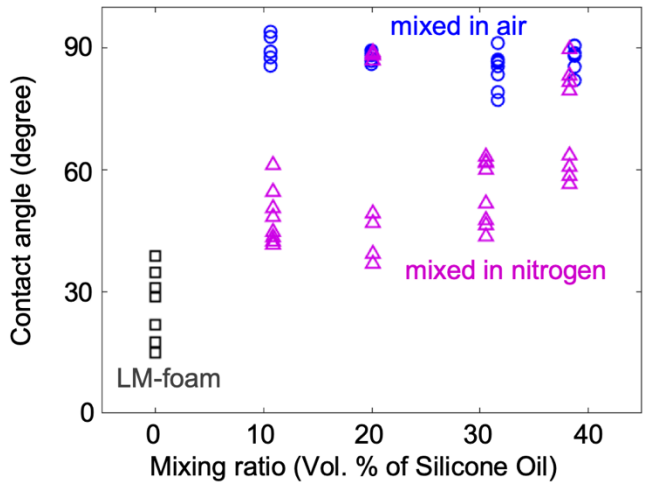

Figure 4.4: Water contact angles measured on the surfaces of the LM foam and its mixtures with silicone oil made in an air (i.e., emulsion) or nitrogen environment as a function of the silicone oil and the LM foam volumetric mixing ratio.

Figure 4.5 presents optical and cryo-FIB-SEM surface and cross-sectional images of the bare LM foam (**a**) as well as LM foam mixed with silicone oil in nitrogen (**b**) and air (**c**) environments.

The LM foam contains 100 nm to 200 µm air capsules and has various surface features, including multiscale wrinkles,[82,83] and 5 µm to 100 µm "open-cell" pores. While the cross-sectional optical image of the LM foam mixed with silicone oil in nitrogen is indistinguishable from that of the original LM foam (Figure 4.5a and b), the presence of oil capsules is clearly visible in the emulsion cross-section (Figure 4.5c). As previously discussed in chapter 3, the amount of internal silicone oil features visible in the cross-sections within these emulsions increases with the mixing ratio of the two fluids (as previously shown in Figure 3.4 for the emulsions made from gallium and in the Appendix-3 for the current emulsions made from eGaIn as a LM).

The electrically insulating nature of the silicone oil facilitates its identification in surface electron micrographs of the cryogenically frozen samples. Upon exposure to the electron beam, the oil surface charges and deflects incoming electrons creating dull-gray to bright-white colors and streaky image sections.[81,84] With this "lens", it can be easily interpreted from the electron micrographs that the surface of the emulsions is covered by a continuous oil film that is only pierced by occasional "islands" of locally elevated LM foam topology. In contrast, the surface of the materials mixed in the nitrogen environment is covered by "puddles" of silicone oil and occasional oil-filled pores. The corresponding sample's near-surface cross-sections exposed using ion beam milling confirm observations from exterior surface imaging. Furthermore, the cross-sectional images show that the silicone oil puddles are very shallow, with a thickness of about 100 nm. In comparison, the continuous liquid film is several times thicker (about 300 to 500 nm).

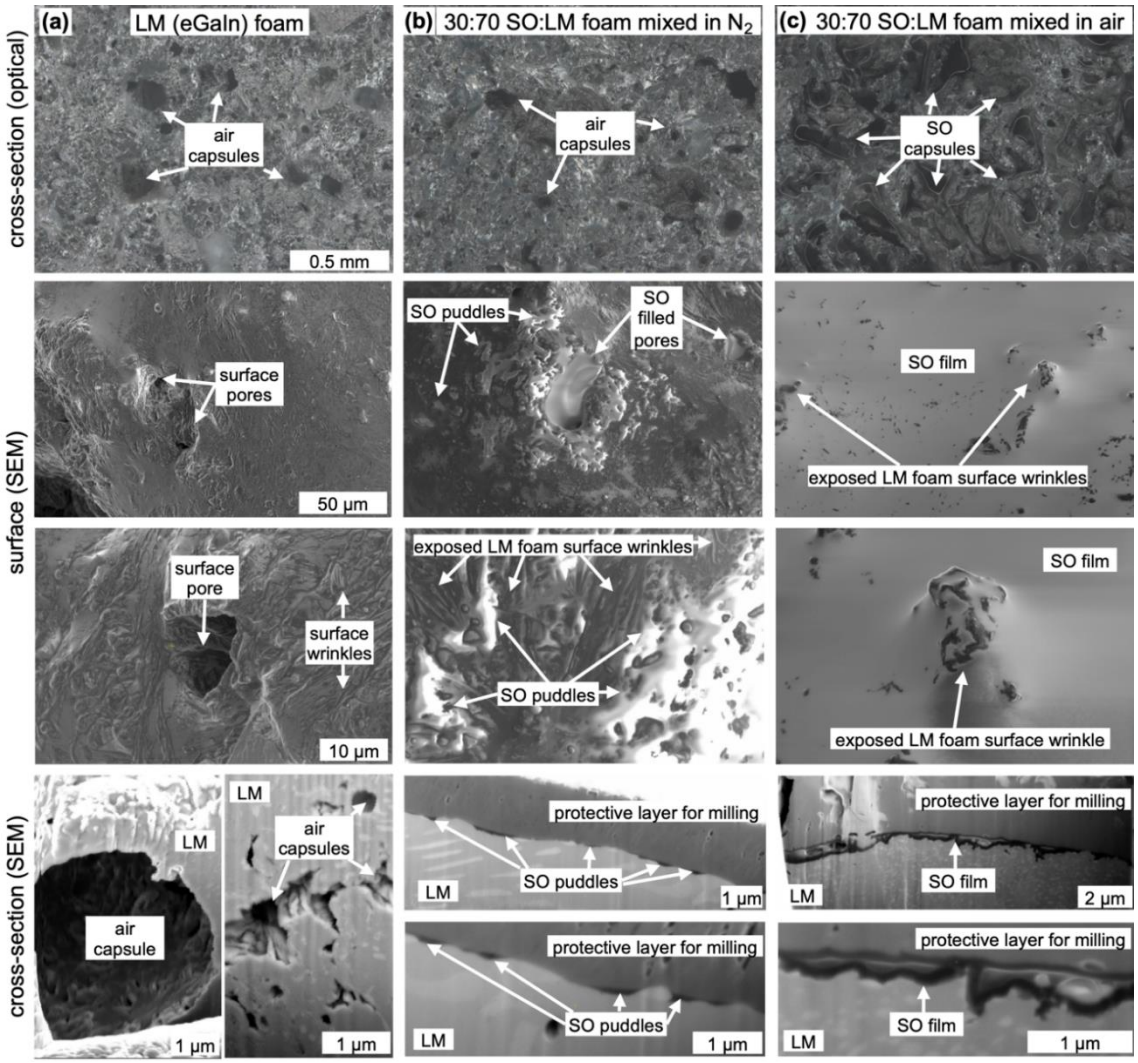

Figure 4.5: Multiscale optical and cryo-FIB-SEM surface and cross-sectional images of (a) the bare LM foam and (b & c) the LM foam mixed with silicone oil (SO) in (b) nitrogen and (c) air environments.

The measured linear decrease in density with mixing volume fraction of silicone oil that was predicted by Eq.8 and the presence of silicone oil in the cross-sectional images provide strong evidence that the emulsions form through incorporation of additional, oxide-covered, liquid capsules. New oxide growth is limited without oxygen in the mixing environment, preventing stable silicone oil capsules and emulsion from forming in nitrogen. Thus, when mixed with the LM foam in nitrogen, the silicone oil only forms

puddles and fills exposed pores on the exterior surface. The minor 5 to 10% density increase is independent of the silicone oil to LM foam mixing ratio in the nitrogen environment because even a small volume of the oil saturates the limited surface features of the foam. It is suspected that in a nitrogen environment, the silicone oil only fills pores and forms puddles on the surface because the lack of oxygen prevents the formation of oxide wrinkles on the LM surface (*i.e.*, oil interacts with a smooth LM surface). In contrast, during mixing in air, the surface waves on the LM surface are preserved in multiscale wrinkles that promote continuous silicone oil film formation.

4.3. Suitability of the Silicone Oil and LM Foam Mixtures for Thermal Interface Materials

Due to their high thermal conductivity and conformability, LMs are increasingly being used as thermal interface materials (TIMs) within the microelectronics industry.[3] However, gallium-based LMs induce corrosion or embrittlement to most metals,[85,86] which requires costly deposition of protective barrier films for LM TIM implementation.[87] This issue can be potentially resolved by the mixed-in-air silicone oil-in-LM foam emulsions.

4.3.1. Prevention of LM-induced Embrittlement of Aluminum Foil

As demonstrated in the previous chapter, the silicone oil-in-gallium foam emulsion (10 cSt with 40% silicone oil) does not embrittle aluminum while at the same time exhibits a moderately high thermal conductivity of about 10 W m^{-1} K^{-1}.[30] The current emulsions with the same 10 cSt silicone oil fraction (made with eGaIn, not pure gallium foam) also do not corrode the foils (as shown in Fig. 4.6a). The cryo-FIB-SEM images confirm the

prior hypothesis that the surface of the emulsions is covered by a continuous layer of silicone oil, which prevents direct LM-aluminum contact. In contrast, such contact and ensuing embrittlement of aluminum are not prevented by the silicone oil puddles on the surface of the materials mixed in a nitrogen environment (Figure 4.6b).

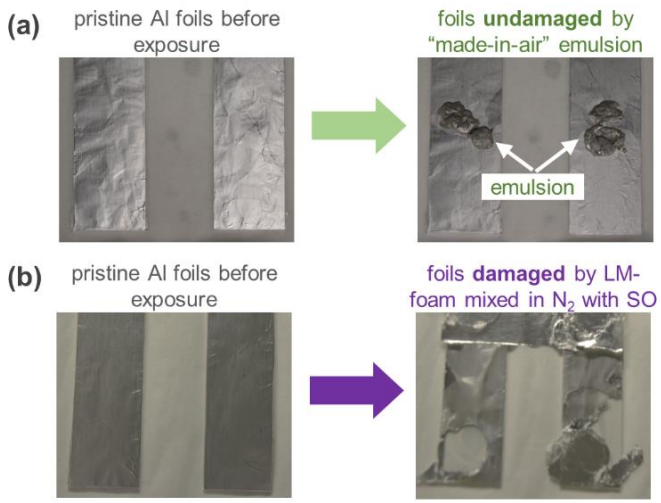

Figure 4.6: Photographs of pristine aluminum foils and those after 24-hour exposure to (a) mixed-in-air silicone oil-in-LM emulsion and the (b) LM-foam mixed with the silicone oil in nitrogen environment

4.3.2. Thermal Conductivity

From a thermal perspective, the conductivity of the current emulsions is similar to the prior results of silicone oil-in-gallium foam emulsion as discussed in chapter 3.[34] In particular, the emulsion effective thermal conductivity steadily decreases with increased silicone oil volume fraction (as shown in Figure 4.7). The effective thermal conductivity of the materials accounts for the intrinsic (*i.e.*, bulk) thermal conductivity of the material as well as for the thermal contact resistances of the two sample-measurement bar interfaces.[51] Consequently, the observed decrease in the effective thermal conductivity can

be attributed to the low thermal conductivity micro-capsules (~0.2 to 0.3 W m^{-1} K^{-1}),[39] whose number increases as the silicone oil volume fraction increases. In contrast, the effective thermal conductivity of the LM foam mixed with silicone oil in nitrogen environments is comparable to or even slightly higher than that of the bare LM foam (around 18 $Wm^{-1}K^{-1}$). This minor effective thermal conductivity increase might stem from the thermal contact resistance reduction by the exterior silicone oil puddles. The continuous silicone oil film on the surface of the emulsions likely also induces a similar or even more significant thermal contact resistance reduction. However, this benefit is negated by decreased intrinsic thermal conductivity associated with silicone oil capsule addition. Consequently, for thermal management applications, the LM foams mixed with silicone oil in a nitrogen environment do not provide any major benefits over bare LM foams. In contrast, the use of the emulsions could remove the need for protective barrier layers, albeit at the cost of reduced thermal conductivity.

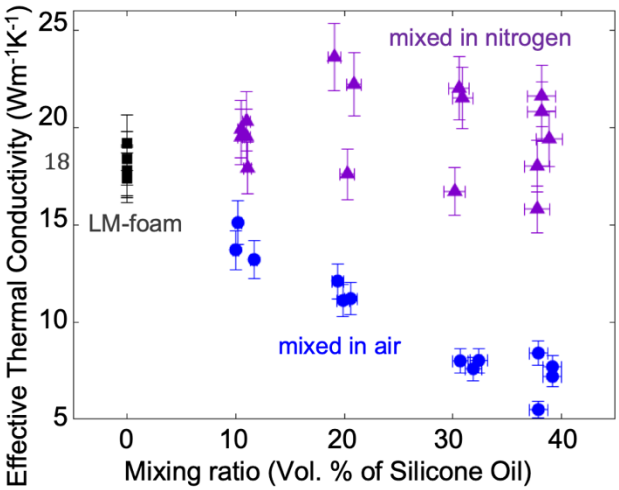

Figure 4.7: The effective thermal conductivity the bare LM foam and the LM foam mixed with silicone oil in nitrogen and air (i.e., the emulsions) environments.

4.4. Conclusion

In summary, this section described two possible mechanisms for the formation of silicone oil-in-LM emulsions and theoretically demonstrated that the dominant mechanism can be distinguished through foam-to-emulsion density change. Specifically, those two mechanisms are: the "replacement mechanism" that consists of silicone oil replacing air features in the LM foam and the "addition mechanism" that consists of silicone oil creating additional features within the LM foam. It was theoretically demonstrated that the former mechanism should be associated with a linear increase in the emulsion density with increasing silicone oil mixing volume fraction, while the latter mechanism should have the opposite effect.

The measurements show that past the 10% oil volume fraction threshold, the density of the emulsions decreases linearly with increasing the silicone oil content. Using multiscale imaging and wettability measurements, it was confirmed that mixing the silicone oil and LM foam in air leads to the incorporation of silicone oil capsules and the formation of emulsions. Consequently, the silicone oil-in-LM emulsions predominantly form by the addition of new silicone oil capsules, as opposed to the replacement of air by the oil in existing foam features.

It was also demonstrated that when silicone oil and LM foam are mixed in a nitrogen environment, there is a small increase in the resulting material density that is independent of the oil volume fraction. By removing oxygen from the mixing environment, the growth of oxide shell on the oil capsules was prevented, which is critical for silicone oil incorporation into the bulk material. Without the oxide growth, cryo-FIB-SEM images revealed that the silicone oil only replaces air within open-cell surface features (*e.g.*, micro-

pores) and forms ~100 nm deep puddles on the LM foam surface. The process leads to a small density increase that is independent of the added volume of silicone oil because there is a limited number of open-cell surface features that are easily saturated by the oil. Interestingly, the surface of the emulsion is covered by a thicker (~300 to 500 nm) and continuous silicone oil film. Its presence explains the lack of density decrease that was observed for the 10% silicone oil volume fraction (i.e., density increases because of the replacement of air in surface features, but its increase is counterbalanced by the addition of silicone capsules into the bulk of the material). It is suspected that mixing of the two fluids in air allows a continuous exterior silicone oil film to form because it promotes continual formation and preservation of multiscale oxide wrinkles. These surface textures do not form on the LM surface during mixing in a nitrogen environment, leading to local dewetting of the silicone oil film. Lastly, it was showed that the continuous silicone oil film on the emulsion surface is necessary to prevent LM-induced embrittlement of contacting aluminum. This unique feature of the silicone oil-in-LM emulsions makes them potential candidates for thermal management applications.

CHAPTER 5

FUTURE WORK

5.1. Summary of Dissertation

Aimed at addressing challenges in industrial processing and application of gallium-based liquid metals (LM), this work introduced two new materials, LM foams and LM emulsions with much improved properties and applicability than the pure LM. I have introduced simple but robust methods for fabrication of these materials that are scalable for industrial processing. Throughout this research, emphasis was placed on uncovering the microscale mechanisms and processes underlying formation of these materials. Their structure-property relationships and example applications were discussed.

The LM foams were investigated to address the challenges of LM's poor adhesion, low viscosity and rapid oxidation that hinder its repeated application to different surfaces and complicate many industrial manufacturing processes. Foaming of liquid gallium was performed by simple shear-mixing the bulk gallium in air, resulting in surface to bulk incorporation of oxides, which in turn stabilize microscale air cavities. This led to a paste-like LM morphology that is easier to spread and apply to industrially relevant surfaces.

The LM foam in turn enabled internalization of a secondary liquid such as silicone oil into the LM structure resulting in a liquid-in-LM (or oil-in-LM) emulsion. It was illustrated that the thermophysical properties of the emulsion can be controlled by tuning a few factors such as viscosity of the secondary liquid, composition, and mixing duration. These emulsions have a lower density, better spread-ability, and do not induce corrosion of other metals as original LM and LM foam.

At a fundamental level, my research investigated the mechanism of foam and emulsion formation. A systematic approach was used to determine the onset of foam formation by studying structure and properties of stirred gallium at regular intervals. This revealed that shear-mixing in air causes surface-to-bulk incorporation of gallium oxide fragments, and, after a critical amount of oxide-fragments is internalized, they start to stabilize air bubbles by encapsulating and oxide-bridging. The oxide features in the LM foam in turn stabilize the secondary liquid capsules resulting in liquid-in-LM emulsion.

In the final section, it was illustrated that the secondary liquid internalization could occur by two possible mechanisms i.e., replacement and addition mechanisms. In the first mechanism, the secondary liquid replaces air in the existing foam features, whereas in the latter mechanism the secondary liquid creates additional features within the LM foam. It was demonstrated that the dominant mechanism can be distinguished by changing the environment of processing from air to nitrogen as well as from foam-to-emulsion density changes. A comprehensive analysis of density, multiscale imaging, and surface wettability were presented. Furthermore, thermal conductivity and prevention of aluminum corrosion was discussion for these materials for TIM application.

In short, this dissertation introduced two new materials, LM foams and LM emulsions, and demonstrated their processing methods, processing-structure-property relations and microscale mechanisms underlying their formation. These results added to the fundamental scientific knowledge about these materials, which sets up a foundation for preparing LM foams, emulsions, and multiphase LM materials with a wide range of fluids and controllable properties.

5.2. On-going Research

As stated previously, the fundamental knowledge of LM foam and emulsion formation sets up a foundation for further development of a wide range of materials with controllable properties. Building upon the knowledge from this work, there are two approaches currently under investigation. Each of these approaches intends to mitigate some of the challenges met by the introduced materials (LM foams and LM emulsions).

The first approach aims at improving the LM foam processing and properties. Previously, LM foams were prepared by a simple shear-mixing method that introduces a lot of heterogenous air-cavities of varying size and shapes. This provides only very little control of the foam structure and properties (*i.e.*, only by controlling the extent of shear-mixing). On the other hand, precisely controlling the quantity and size of air bubbles in the LM would provide a homogeneous foam material with controllable properties. A potential pathway to achieve this is by foaming the LM with a decomposition agent. This approach has previously been utilized for foaming of high temperature metal foams[45] as well as room-temperature gallium alloys[31]. A decomposition agent such as sodium bicarbonate ($NaHCO_3$) would decompose upon heating to release gases (CO_2 and H_2O) within the LM, resulting in LM foam formation. To control the foam structure and properties, several control knobs would be available. The particle size and quantity of the decomposition agent may be controlled prior to mixing with the LM, whereas controlling the rate and extent of heating (*i.e.*, temperature) during the foaming process would provide additional controls for the foaming mechanism. The resulting foam is expected to provide a better fit for many

industrial applications such as wearable electronics, stretchable devices, and biomedical applications etc.

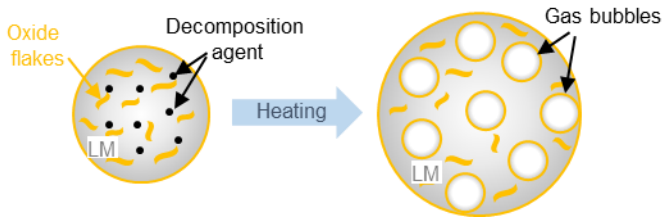

Figure 5.1: Foaming of LM using decomposition agents

The second approach aims at improving the LM emulsions' thermal conductivity for TIM application. Previously, the emulsions were prepared by mixing the LM foam with a secondary liquid such as silicone oil. The silicone oil provides lubrication and a barrier layer against LM-induced corrosion of other metal surfaces such aluminum under elevated temperature and mild pressure typical of TIM applications. However, the resulting emulsion consists of around 50% by volume of insulating air cavities and silicone oil features, hindering thermal transport and thereby lowering the LM's thermal conductivity by two thirds. This loss in thermal transport may be mitigated by two ways, first by reducing the overall disruption to the thermal percolation by reducing the overall content of insulating materials (*i.e.*, air-cavities and oil), and second by introducing conductive solid particles.

The previous section on emulsion formation mechanism demonstrated that secondary liquid incorporates into the LM by the 'addition' mechanism. This suggests that prior foaming of the LM is not necessary as long the LM possesses sufficient oxide features, and it is viscous enough to stabilize secondary liquid capsules (*i.e.*, prevent coalescence and buoyancy-driven escape). This inference can potentially be realized by

mixing the secondary liquid with a LM-paste with no or little foam content, but consisting of a conductive solid material and viscous enough to stabilize the secondary liquid capsules. Such a LM-paste can be made by shear-mixing the LM with an inert conductive powder such as silica or silicon carbide using a mortar and pestle. However, it may be challenging to find the desired LM-paste with just the right structure and composition to enable emulsion formation. Nevertheless, this direction of research may lead to truly multiphase LM pastes having significantly higher thermal conductivity and wider property tunability than the current LM foam and emulsions.

5.3. Future Directions

This work can lead to several future directions. One direction can be exploring various fluid options or the use of multiple fluids for preparing liquid-in-LM emulsions to expand their characteristics and to enable many industry-specific needs. The research in this dissertation was limited to LM-emulsion using just one fluid type (*i.e.*, silicone oil), besides requiring a pre-foamed LM material to start with. Preparing a silicone oil-in-LM emulsion benefits from plenty of dissolved oxygen in the silicone oil, which other fluids may lack. Whereas the limitation of using a pre-foamed LM arises from high surface tension of pure LM which causes the LM to take the dispersed phase in other liquids to minimize its surface free energy. To prepare liquid-in-LM emulsions using desired fluids, these challenges must be overcome using innovative ways. An idea would be to explore emulsifying agents for LM systems like those used for other immiscible systems such as the oil and water system.

Emulsifying agents reduce the interfacial tension between the dispersed and continuous phases in an emulsion thereby imparting kinetic stability to the emulsion. They can adsorb to the interface of the disperse phase droplets, forming an oriented monolayer. A recent study used sodium dodecyl sulphate (SDS), an anionic surfactant for forming liquid metal vacuoles that are bubble-like two-dimensional liquid metals structures.[88] Other than SDS, several other surfactants can be explored such as oleic acid, capric acid or gemini surfactants. Besides emulsifying agents, colloidal solid particles like those used in Pickering emulsions[35] can be explored for stabilizing the LM emulsion.

Another direction can be exploring the possibility of direct injection of the secondary fluids (liquids and gases) into the LM pastes to prepare LM foams and emulsions with controlled structure and properties. Direction injection of gases is also used for production of metal foams such as using aluminum alloys. However, our initial efforts to utilize this methodology did not work due to challenges in controlling droplet size, buoyancy-driven flow, and coalescence of disperse phase droplets. Nevertheless, once suitable emulsifying agents for LM systems are established, this approach may be revisited.

5.4. Preliminary Experiments of Using Oleic Acid as Surfactant

Preparing LM-emulsion without excessive air pockets and oxide content is desired to improve its properties. Therefore, preliminary experiments were performed to find if adding a surfactant to secondary liquid (silicone oil, SO) can improve its emulsification with the LM or LM foam. Oleic acid (OA, technical grade 90% by Sigma Aldrich) was selected as a surfactant since it’s non-toxic and readily available in nature. To observe if OA improves the emulsion formation of SO with the LM, several experiments were

performed to mix LM or LM foam with one of the three different liquids (pure 10cSt SO, a mixture of 3% OA in SO, or pure OA).

First, LM (eGaIn)-foam was mixed with each of the above three liquids in the air for 15 minutes (Fig. 5.2 a-c). In each case, the liquid completely internalized into the LM-foam in 10-12 minutes forming a liquid-in-LM emulsion. No significant difference was observed visually among the three liquids for emulsion formation.

Next, the same experiments of mixing LM-foam with each of the three liquids were repeated in an oxygen-deprived environment (nitrogen-filled glove bag) (Fig. 5.2 d-f). In this case, no emulsion formation occurred and plenty of liquid was unmixed after 15-minutes of mixing. This is due to lack of oxygen necessary for emulsion formation as discussed in chapter 4. Again, no difference was observed among SO, OA or a mixture of SO and OA for emulsion formation in nitrogen.

Finally, pure LM (Ga) was mixed with each of the same three liquids for 5 minutes in air (Fig. 5.2 g-i). Pure LM divides into smaller droplets when mixed with other liquids in air due to its high cohesive energy density. However, in this case OA acted slightly differently than the SO. In case of SO (as well as mixture of OA in SO), the LM divides into many droplets of varying sizes (from mm to µm scale). These droplets are prevented from coalescence by oxide shells, that rapidly form around exposed gallium surface due to dissolved oxygen in the SO. In contrast, when mixing LM with pure OA, only the tiniest LM droplets are seen, whereas the larger (*e.g.*, 1 mm sized) droplets do not form. Lack of oxide shell formation is also visible when two or more LM drops form while shearing, but then soon coalesce back into a single LM blob. This is likely due to two reasons: (i) a lack of dissolved oxygen in the OA and (ii) the likely presence

of a surface-bound monolayer oleic acid that slows and/or inhibits dissolved oxygen from getting to the LM surface.

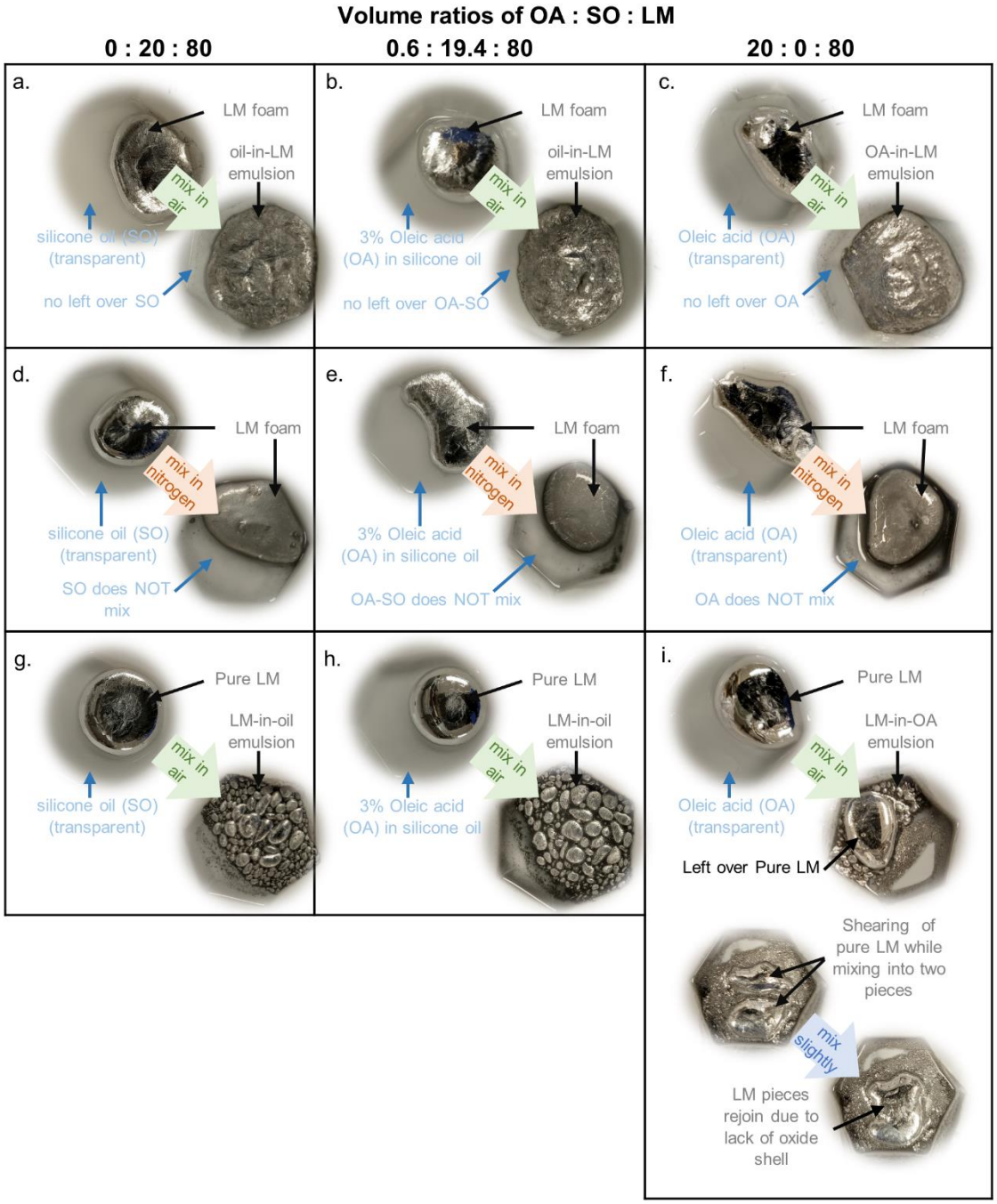

Figure 5.2: Using Oleic acid as surfactant: mixing LM-foam with SO and OA in air (a-c), and nitrogen (d-f) environments, (g-i) mixing pure LM with SO and OA in air

From these ‘limited observations’, it is found that adding OA to the SO does not improve its emulsion formation with the LM foam. Though the OA can bond to the metal surface by its carboxylic group, this bonding mechanism is not sufficient for emulsion formation in oxygen-free environment. It is noted that the pure LM always forms dispersed LM droplets even when high volume ratio of LM is used. Unlike oil-and-water systems, which can be easily emulsified using surfactants, LMs may be difficult to emulsify due to their unique characteristics (metallic bonding, high surface tension, high density difference and rapid surface oxidation etc.). Besides, it may be noted that the relative miscibility of surfactant in oil or water systems (such as Winsor I and II type) affects which liquid takes the continuous phase[38,66,89]. Therefore, a surfactant that is soluble in LM (unlike OA which is soluble in the oil) may have a better chance of forming an emulsion with LM as a continuous phase. Since most liquids are non-soluble with the LM, trying solid particles (such as SiO_2) as surfactant to form a Pickering emulsion seems a good approach for future experiments.

REFERENCES

(1) Handschuh-Wang, S.; Stadler, F. J.; Zhou, X. Critical Review on the Physical Properties of Gallium-Based Liquid Metals and Selected Pathways for Their Alteration. *J. Phys. Chem. C* **2021**, *125* (37), 20113–20142. https://doi.org/10.1021/acs.jpcc.1c05859.

(2) Bernhoft, R. A. Mercury Toxicity and Treatment: A Review of the Literature. *J. Environ. Public Health* **2012**, *2012*, 1–10. https://doi.org/10.1155/2012/460508.

(3) Chen, S.; Deng, Z.; Liu, J. High Performance Liquid Metal Thermal Interface Materials. *Nanotechnology* **2021**, *32* (9), 092001. https://doi.org/10.1088/1361-6528/abcbc2.

(4) Kong, W.; Wang, Z.; Wang, M.; Manning, K. C.; Uppal, A.; Green, M. D.; Wang, R. Y.; Rykaczewski, K. Oxide-Mediated Formation of Chemically Stable Tungsten–Liquid Metal Mixtures for Enhanced Thermal Interfaces. *Adv. Mater.* **2019**, *31* (44), 1904309. https://doi.org/10.1002/adma.201904309.

(5) Wang, X.; Guo, R.; Liu, J. Liquid Metal Based Soft Robotics: Materials, Designs, and Applications. *Adv. Mater. Technol.* **2019**, *4* (2), 1800549. https://doi.org/10.1002/admt.201800549.

(6) Teng, L.; Ye, S.; Handschuh-Wang, S.; Zhou, X.; Gan, T.; Zhou, X. Liquid Metal-Based Transient Circuits for Flexible and Recyclable Electronics. *Adv. Funct. Mater.* **2019**, *29* (11), 1808739. https://doi.org/10.1002/adfm.201808739.

(7) Ilyas, N.; Cook, A.; Tabor, C. E. Designing Liquid Metal Interfaces to Enable Next Generation Flexible and Reconfigurable Electronics. *Adv. Mater. Interfaces* **2017**, *4* (15), 1700141. https://doi.org/10.1002/admi.201700141.

(8) Chechetka, S. A.; Yu, Y.; Zhen, X.; Pramanik, M.; Pu, K.; Miyako, E. Light-Driven Liquid Metal Nanotransformers for Biomedical Theranostics. *Nat. Commun.* **2017**, *8* (1), 15432. https://doi.org/10.1038/ncomms15432.

(9) Wang, B.; Facchetti, A. Mechanically Flexible Conductors for Stretchable and Wearable E-Skin and E-Textile Devices. *Adv. Mater.* **2019**, *31* (28), 1901408. https://doi.org/10.1002/adma.201901408.

(10) Wang, X.; Yao, W.; Guo, R.; Yang, X.; Tang, J.; Zhang, J.; Gao, W.; Timchenko, V.; Liu, J. Soft and Moldable Mg-Doped Liquid Metal for Conformable Skin Tumor Photothermal Therapy. *Adv. Healthc. Mater.* **2018**, *7* (14), 1800318. https://doi.org/10.1002/adhm.201800318.

(11) Daalkhaijav, U.; Yirmibesoglu, O. D.; Walker, S.; Mengüç, Y. Rheological Modification of Liquid Metal for Additive Manufacturing of Stretchable Electronics. *Adv. Mater. Technol.* **2018**, *3* (4), 1700351. https://doi.org/10.1002/admt.201700351.

(12) Markvicka, E. J.; Bartlett, M. D.; Huang, X.; Majidi, C. An Autonomously Electrically Self-Healing Liquid Metal–Elastomer Composite for Robust Soft-Matter Robotics and Electronics. *Nat. Mater.* **2018**, *17* (7), 618–624. https://doi.org/10.1038/s41563-018-0084-7.

(13) Kamdar, M. H. Liquid Metal Embrittlement. In *Treatise on Materials Science & Technology*; Elsevier, 1983; Vol. 25, pp 361–459. https://doi.org/10.1016/B978-0-12-341825-8.50015-5.

(14) Deng, Y.-G.; Liu, J. Corrosion Development between Liquid Gallium and Four Typical Metal Substrates Used in Chip Cooling Device. *Appl. Phys. A* **2009**, *95* (3), 907–915. https://doi.org/10.1007/s00339-009-5098-1.

(15) Cui, Y.; Ding, Y.; Xu, S.; Yang, Z.; Zhang, P.; Rao, W.; Liu, J. Liquid Metal Corrosion Effects on Conventional Metallic Alloys Exposed to Eutectic Gallium–Indium Alloy Under Various Temperature States. *Int. J. Thermophys.* **2018**, *39* (10), 113. https://doi.org/10.1007/s10765-018-2440-x.

(16) Senel, E.; Walmsley, J. C.; Diplas, S.; Nisancioglu, K. Liquid Metal Embrittlement of Aluminium by Segregation of Trace Element Gallium. *Corros. Sci.* **2014**, *85*, 167–173. https://doi.org/10.1016/j.corsci.2014.04.012.

(17) Uppal, A.; Kong, W.; Rana, A.; Wang, R. Y.; Rykaczewski, K. Enhancing Thermal Transport in Silicone Composites via Bridging Liquid Metal Fillers with Reactive Metal Co-Fillers and Matrix Viscosity Tuning. *ACS Appl. Mater. Interfaces* **2021**, *13* (36), 43348–43355. https://doi.org/10.1021/acsami.1c11275.

(18) Tang, J.; Zhao, X.; Li, J.; Guo, R.; Zhou, Y.; Liu, J. Gallium-Based Liquid Metal Amalgams: Transitional-State Metallic Mixtures (TransM ^{2} Ixes) with Enhanced and Tunable Electrical, Thermal, and Mechanical Properties. *ACS Appl. Mater. Interfaces* **2017**, *9* (41), 35977–35987. https://doi.org/10.1021/acsami.7b10256.

(19) Tang, J.; Zhao, X.; Li, J.; Zhou, Y.; Liu, J. Liquid Metal Phagocytosis: Intermetallic Wetting Induced Particle Internalization. *Adv. Sci.* **2017**, *4* (5), 1700024. https://doi.org/10.1002/advs.201700024.

(20) Lin, Z.; Liu, H.; Li, Q.; Liu, H.; Chu, S.; Yang, Y.; Chu, G. High Thermal Conductivity Liquid Metal Pad for Heat Dissipation in Electronic Devices. *Appl. Phys. A* **2018**, *124* (5), 368. https://doi.org/10.1007/s00339-018-1778-z.

(21) Tavakoli, M.; Malakooti, M. H.; Paisana, H.; Ohm, Y.; Marques, D. G.; Lopes, P. A.; Piedade, A. P.; Almeida, A. T. de; Majidi, C. Stretchable Electronics: EGaIn-Assisted Room-Temperature Sintering of Silver Nanoparticles for Stretchable, Inkjet-Printed, Thin-Film Electronics (Adv. Mater. 29/2018). *Adv. Mater.* **2018**, *30* (29), 1870215. https://doi.org/10.1002/adma.201870215.

(22) Wei, S.; Yu, Z. F.; Zhou, L. J.; Guo, J. D. Investigation on Enhancing the Thermal Conductance of Gallium-Based Thermal Interface Materials Using Chromium-Coated Diamond Particles. *J. Mater. Sci. Mater. Electron.* **2019**, *30* (7), 7194–7202. https://doi.org/10.1007/s10854-019-01038-0.

(23) Kong, W.; Wang, Z.; Casey, N.; Korah, M. M.; Uppal, A.; Green, M. D.; Rykaczewski, K.; Wang, R. Y. High Thermal Conductivity in Multiphase Liquid Metal and Silicon Carbide Soft Composites. *Adv. Mater. Interfaces* **2021**, *8* (14), 2100069. https://doi.org/10.1002/admi.202100069.

(24) Sargolzaeiaval, Y.; Ramesh, V. P.; Neumann, T. V.; Miles, R.; Dickey, M. D.; Öztürk, M. C. High Thermal Conductivity Silicone Elastomer Doped with Graphene Nanoplatelets and Eutectic GaIn Liquid Metal Alloy. *ECS J. Solid State Sci. Technol.* **2019**, *8* (6), P357–P362. https://doi.org/10.1149/2.0271906jss.

(25) Bartlett, M. D.; Kazem, N.; Powell-Palm, M. J.; Huang, X.; Sun, W.; Malen, J. A.; Majidi, C. High Thermal Conductivity in Soft Elastomers with Elongated Liquid Metal Inclusions. *Proc. Natl. Acad. Sci.* **2017**, *114* (9), 2143–2148. https://doi.org/10.1073/pnas.1616377114.

(26) Ralphs, M.; Kong, W.; Wang, R. Y.; Rykaczewski, K. Thermal Conductivity Enhancement of Soft Polymer Composites through Magnetically Induced Percolation and Particle–Particle Contact Engineering. *Adv. Mater. Interfaces* **2019**, *6* (6), 1801857. https://doi.org/10.1002/admi.201801857.

(27) Ralphs, M. I.; Kemme, N.; Vartak, P. B.; Joseph, E.; Tipnis, S.; Turnage, S.; Solanki, K. N.; Wang, R. Y.; Rykaczewski, K. In Situ Alloying of Thermally Conductive Polymer Composites by Combining Liquid and Solid Metal Microadditives. *ACS Appl. Mater. Interfaces* **2018**, *10* (2), 2083–2092. https://doi.org/10.1021/acsami.7b15814.

(28) Uppal, A.; Ralphs, M.; Kong, W.; Hart, M.; Rykaczewski, K.; Wang, R. Y. Pressure-Activated Thermal Transport via Oxide Shell Rupture in Liquid Metal Capsule Beds. *ACS Appl. Mater. Interfaces* **2020**, *12* (2), 2625–2633. https://doi.org/10.1021/acsami.9b17358.

(29) Chen, S.; Wang, H.-Z.; Zhao, R.-Q.; Rao, W.; Liu, J. Liquid Metal Composites. *Matter* **2020**, *2* (6), 1446–1480. https://doi.org/10.1016/j.matt.2020.03.016.

(30) Shah, N. U. H.; Kong, W.; Casey, N.; Kanetkar, S.; Wang, R. Y.; Rykaczewski, K. Gallium Oxide-Stabilized Oil in Liquid Metal Emulsions. *Soft Matter* **2021**, *17* (36), 8269–8275. https://doi.org/10.1039/D1SM00982F.

(31) Gao, J.; Ye, J.; Chen, S.; Gong, J.; Wang, Q.; Liu, J. Liquid Metal Foaming via Decomposition Agents. *ACS Appl. Mater. Interfaces* **2021**, *13* (14), 17093–17103. https://doi.org/10.1021/acsami.1c01731.

(32) Zhang, M.; Liu, L.; Zhang, C.; Chang, H.; Zhang, P.; Rao, W. Self-Foaming as a Universal Route for Fabricating Liquid Metal Foams and Hollow Particles. *Adv. Mater. Interfaces* **2021**, *8* (12), 2100432. https://doi.org/10.1002/admi.202100432.

(33) Wang, X.; Fan, L.; Zhang, J.; Sun, X.; Chang, H.; Yuan, B.; Guo, R.; Duan, M.; Liu, J. Printed Conformable Liquid Metal E-Skin-Enabled Spatiotemporally Controlled Bioelectromagnetics for Wireless Multisite Tumor Therapy. *Adv. Funct. Mater.* **2019**, *29* (51), 1907063. https://doi.org/10.1002/adfm.201907063.

(34) Yang, J.; Tang, D.; Ao, J.; Ghosh, T.; Neumann, T. V.; Zhang, D.; Piskarev, E.; Yu, T.; Truong, V. K.; Xie, K.; Lai, Y.-C.; Li, Y.; Dickey, M. D. Ultrasoft Liquid Metal Elastomer Foams with Positive and Negative Piezopermittivity for Tactile Sensing. *Adv. Funct. Mater.* **2020**, *n/a* (n/a), 2002611. https://doi.org/10.1002/adfm.202002611.

(35) Pickering, S. U. CXCVI.—Emulsions. *J. Chem. Soc. Trans.* **1907**, *91* (0), 2001–2021. https://doi.org/10.1039/CT9079102001.

(36) Asadabadi, M. R.; Abolghasemi, H.; Maragheh, M. G.; Nasab, P. D. Effect of Silica Nanoparticles on the Phase Inversion of Liquid-Liquid Dispersions. *Korean J. Chem. Eng.* **2013**, *30* (3), 733–738. https://doi.org/10.1007/s11814-012-0195-9.

(37) Perazzo, A.; Preziosi, V.; Guido, S. Phase Inversion Emulsification: Current Understanding and Applications. *Adv. Colloid Interface Sci.* **2015**, *222*, 581–599. https://doi.org/10.1016/j.cis.2015.01.001.

(38) Tadros, T. F. *Emulsions : Formation, Stability, Industrial Applications*; Walter de Gruyter GmbH: Berlin/Boston, GERMANY, 2016.

(39) Kong, W.; Wang, Z.; Wang, M.; Manning, K. C.; Uppal, A.; Green, M. D.; Wang, R. Y.; Rykaczewski, K. Oxide-Mediated Formation of Chemically Stable Tungsten-Liquid Metal Mixtures for Enhanced Thermal Interfaces. *Adv. Mater.* **2019**, *31* (44), 1904309.

(40) Daalkhaijav, U.; Yirmibesoglu, O. D.; Walker, S.; Mengüç, Y. Rheological Modification of Liquid Metal for Additive Manufacturing of Stretchable Electronics: Supporting Information. *Adv. Mater. Technol.* **2018**, *3* (4), 1700351. https://doi.org/10.1002/admt.201700351.

(41) Wang, X.; Fan, L.; Zhang, J.; Sun, X.; Chang, H.; Yuan, B.; Guo, R.; Duan, M.; Liu, J. Printed Conformable Liquid Metal E-Skin-Enabled Spatiotemporally Controlled Bioelectromagnetics for Wireless Multisite Tumor Therapy. *Adv. Funct. Mater.* **2019**, 1907063.

(42) Chang, H.; Guo, R.; Sun, Z.; Wang, H.; Hou, Y.; Wang, Q.; Rao, W.; Liu, J. Direct Writing and Repairable Paper Flexible Electronics Using Nickel–Liquid Metal Ink. *Adv. Mater. Interfaces* **2018**, *5*, 1800571. https://doi.org/10.1002/admi.201800571.

(43) Wang, H.; Yuan, B.; Liang, S.; Guo, R.; Rao, W.; Wang, X.; Chang, H.; Ding, Y.; Liu, J.; Wang, L. Plus-M: A Porous Liquid-Metal Enabled Ubiquitous Soft Material. *Mater. Horiz.* **2018**, *5* (2), 222–229.

(44) Yuan, B.; Zhao, C.; Sun, X.; Liu, J. Lightweight Liquid Metal Entity. *Adv. Funct. Mater.* **2020**, 1910709.

(45) Banhart, J. Metal Foams: Production and Stability. *Adv. Eng. Mater.* **2006**, *8* (9), 781–794. https://doi.org/10.1002/adem.200600071.

(46) Farrell, Z. J.; Tabor, C. Control of Gallium Oxide Growth on Liquid Metal Eutectic Gallium/Indium Nanoparticles via Thiolation. *Langmuir* **2018**, *34* (1), 234–240. https://doi.org/10.1021/acs.langmuir.7b03384.

(47) Liu, S.; Sun, X.; Kemme, N.; Damle, V. G. G.; Schott, C.; Herrmann, M.; Rykaczewski, K. Can Liquid Metal Flow in Microchannels Made of Its Own Oxide Skin? *Microfluid. Nanofluidics* **2016**, *20* (1), 1–6.

(48) Doudrick, K.; Liu, S.; Mutunga, E. M. E. M.; Klein, K. L. K. L.; Damle, V.; Varanasi, K. K. K.; Rykaczewski, K. Different Shades of Oxide: From Nanoscale Wetting Mechanisms to Contact Printing of Gallium-Based Liquid Metals. *Langmuir* **2014**, *30* (23), 6867–6877. https://doi.org/10.1021/la5012023.

(49) Plech, A.; Klemradt, U.; Metzger, H.; Peisl, J. In Situ X-Ray Reflectivity Study of the Oxidation Kinetics of Liquid Gallium and the Liquid Alloy. *J. Phys. Condens. Matter* **1998**, *10* (5), 971.

(50) Chabala, J. M. Oxide-Growth Kinetics and Fractal-like Patterning across Liquid Gallium Surfaces. *Phys. Rev. B* **1992**, *46* (18), 11346.

(51) Chen, Y.; Wagner, J. L.; Farias, P. A.; DeMauro, E. P.; Guildenbecher, D. R. Galinstan Liquid Metal Breakup and Droplet Formation in a Shock-Induced Cross-Flow. *Int. J. Multiph. Flow* **2018**, *106*, 147–163.

(52) Antoniou, N.; Rykaczewski, K.; Uchic, M. D. In Situ FIB-SEM Characterization and Manipulation Methods. *MRS Bull.* **2014**, *39* (04), 347–352.

(53) Rykaczewski, K.; Anand, S.; Subramanyam, S. B. S. B.; Varanasi, K. K. K. Mechanism of Frost Formation on Lubricant-Impregnated Surfaces. *Langmuir* **2013**, *29* (17), 5230–5238. https://doi.org/10.1021/la400801s.

(54) Spierings, A. B.; Schneider, M.; Eggenberger, R. Comparison of Density Measurement Techniques for Additive Manufactured Metallic Parts. *Rapid Prototyp. J.* **2011**, *17* (5), 380–386. https://doi.org/10.1108/13552541111156504.

(55) Regan, M. J.; Pershan, P. S.; Magnussen, O. M.; Ocko, B. M.; Deutsch, M.; Berman, L. E. X-Ray Reflectivity Studies of Liquid Metal and Alloy Surfaces. *Phys. Rev. B* **1997**, *55* (23), 15874–15884. https://doi.org/10.1103/PhysRevB.55.15874.

(56) Bayraktaroglu, B. Assessment of Gallium Oxide Technology. *Air Force Res. Lab. Sens. Dir. WPAFB U. S.* **2017**, *No. AFRL-R*, 1–103.

(57) Thompson, D. R.; Rao, S. R.; Cola, B. A. A Stepped-Bar Apparatus for Thermal Resistance Measurements. *J. Electron. Packag.* **2013**, *135* (4), 41002.

(58) Ralphs, M.; Kong, W.; Wang, R. Y.; Rykaczewski, K. Thermal Conductivity Enhancement of Soft Polymer Composites through Magnetically Induced Percolation and Particle–Particle Contact Engineering. *Adv. Mater. Interfaces* **2019**, *6* (6), 1801857. https://doi.org/10.1002/admi.201801857.

(59) Bartlett, M. D.; Kazem, N.; Powell-Palm, M. J.; Huang, X.; Sun, W.; Malen, J. A.; Majidi, C. High Thermal Conductivity in Soft Elastomers with Elongated Liquid Metal Inclusions. *Proc. Natl. Acad. Sci.* **2017**, *114* (9), 2143–2148.

(60) Ralphs, M. I.; Kemme, N.; Vartak, P. B.; Joseph, E.; Tipnis, S.; Turnage, S.; Solanki, K. N.; Wang, R. Y.; Rykaczewski, K. In Situ Alloying of Thermally Conductive Polymer Composites by Combining Liquid and Solid Metal Microadditives. *ACS Appl. Mater. Interfaces* **2018**, *10* (2), 2083–2092. https://doi.org/10.1021/acsami.7b15814.

(61) Tutika, R.; Zhou, S. H.; Napolitano, R. E.; Bartlett, M. D. Mechanical and Functional Tradeoffs in Multiphase Liquid Metal, Solid Particle Soft Composites. *Adv. Funct. Mater.* **2018**, 1804336.

(62) Tan, M. C.; Chin, N. L.; Yusof, Y. A.; Taip, F. S.; Abdullah, J. Characterisation of Improved Foam Aeration and Rheological Properties of Ultrasonically Treated Whey Protein Suspension. *Int. Dairy J.* **2015**, *43*, 7–14.

(63) Körner, C.; Arnold, M.; Singer, R. F. Metal Foam Stabilization by Oxide Network Particles. *Mater. Sci. Eng. A* **2005**, *396* (1–2), 28–40.

(64) Banhart, J. Metal Foams: Production and Stability. *Adv. Eng. Mater.* **2006**, *8* (9), 781–794.

(65) Xu, Q.; Oudalov, N.; Guo, Q.; Jaeger, H. M.; Brown, E. Effect of Oxidation on the Mechanical Properties of Liquid Gallium and Eutectic Gallium-Indium. *Phys. Fluids* **2012**, *24* (6), 1–13. https://doi.org/10.1063/1.4724313.

(66) Perazzo, A.; Preziosi, V.; Guido, S. Phase Inversion Emulsification: Current Understanding and Applications. *Adv. Colloid Interface Sci.* **2015**, *222*, 581–599. https://doi.org/10.1016/j.cis.2015.01.001.

(67) Kumar, A.; Li, S.; Cheng, C. M.; Lee, D. Recent Developments in Phase Inversion Emulsification. *Ind. Eng. Chem. Res.* **2015**, *54* (34), 8375–8396. https://doi.org/10.1021/acs.iecr.5b01122.

(68) Tutika, R.; Kmiec, S.; Haque, A. B. M. T.; Martin, S. W.; Bartlett, M. D. Liquid Metal–Elastomer Soft Composites with Independently Controllable and Highly Tunable Droplet Size and Volume Loading. *ACS Appl. Mater. Interfaces* **2019**, *11* (19), 17873–17883. https://doi.org/10.1021/acsami.9b04569.

(69) Koh, A.; Sietins, J.; Slipher, G.; Mrozek, R. Deformable Liquid Metal Polymer Composites with Tunable Electronic and Mechanical Properties. *J. Mater. Res.* **2018**, *33* (17), 2443–2453. https://doi.org/10.1557/jmr.2018.209.

(70) Ralphs, M. I. M. I.; Kemme, N.; Vartak, P. B. P. B.; Joseph, E.; Tipnis, S.; Turnage, S.; Solanki, K. N.; Wang, R. Y. R. Y. R. Y.; Rykaczewski, K. In Situ Alloying of Thermally Conductive Polymer Composites by Combining Liquid and Solid Metal Microadditives. *ACS Appl. Mater. Interfaces* **2018**, *10* (2), 2083–2092. https://doi.org/10.1021/acsami.7b15814.

(71) Kong, W.; Shah, N. U. H.; Neumann, T. V.; Vong, M. H.; Kotagama, P.; Dickey, M. D.; Wang, R. Y.; Rykaczewski, K. Oxide-Mediated Mechanisms of Gallium Foam Generation and Stabilization during Shear Mixing in Air. *Soft Matter* **2020**, *16* (25), 5801–5805. https://doi.org/10.1039/D0SM00503G.

(72) Kempers, R.; Kolodner, P.; Lyons, A.; Robinson, A. J. A High-Precision Apparatus for the Characterization of Thermal Interface Materials. *Rev. Sci. Instrum.* **2009**, *80* (9), 1–11. https://doi.org/10.1063/1.3193715.

(73) Kong, W.; Wang, Z.; Wang, M.; Manning, K. C.; Uppal, A.; Green, M. D.; Wang, R. Y.; Rykaczewski, K. Oxide-Mediated Formation of Chemically Stable Tungsten–Liquid Metal Mixtures for Enhanced Thermal Interfaces. *Adv. Mater.* **2019**, *31* (44), 1904309. https://doi.org/10.1002/adma.201904309.

(74) Fukuyama, H.; Yoshimura, T.; Yasuda, H.; Ohta, H. Thermal Conductivity Measurements of Liquid Mercury and Gallium by a Transient Hot-Wire Method in a Static Magnetic Field. *Int. J. Thermophys.* **2006**, *27* (6), 1760–1777.

(75) Anand, S.; Rykaczewski, K.; Subramanyam, S. B.; Beysens, D.; Varanasi, K. K. How Droplets Nucleate and Grow on Liquids and Liquid Impregnated Surfaces. *Soft Matter* **2015**, *11* (1), 69–80. https://doi.org/10.1039/C4SM01424C.

(76) Damle, V. G.; Tummala, A.; Chandrashekar, S.; Kido, C.; Roopesh, A.; Sun, X.; Doudrick, K.; Chinn, J.; Lee, J. R.; Burgin, T. P.; Rykaczewski, K. "Insensitive" to Touch: Fabric-Supported Lubricant-Swollen Polymeric Films for Omniphobic Personal Protective Gear. *ACS Appl. Mater. Interfaces* **2015**, *7* (7), 4224–4232. https://doi.org/10.1021/am5085226.

(77) Smith, J. D.; Dhiman, R.; Anand, S.; Reza-Garduno, E.; Cohen, R. E.; McKinley, G. H.; Varanasi, K. K. Droplet Mobility on Lubricant-Impregnated Surfaces. *Soft Matter* **2013**, *9* (6), 1772–1780. https://doi.org/10.1039/C2SM27032C.

(78) Boreyko, J. B.; Polizos, G.; Datskos, P. G.; Sarles, S. A.; Collier, C. P. Air-Stable Droplet Interface Bilayers on Oil-Infused Surfaces. *Proc. Natl. Acad. Sci.* **2014**, *111* (21), 7588–7593.

(79) Yuan, B.; Sun, X.; Wang, H.; Liu, J. Liquid Metal Bubbles. *Appl. Mater. Today* **2021**, *24*, 101151. https://doi.org/10.1016/j.apmt.2021.101151.

(80) Rykaczewski, K.; Landin, T.; Walker, M. L.; Scott, J. H. J.; Varanasi, K. K. Direct Imaging of Complex Nano- to Microscale Interfaces Involving Solid, Liquid, and Gas Phases. *ACS Nano* **2012**, *6* (10), 9326–9334. https://doi.org/10.1021/nn304250e.

(81) Rykaczewski, K.; Anand, S.; Subramanyam, S. B.; Varanasi, K. K. Mechanism of Frost Formation on Lubricant-Impregnated Surfaces. *Langmuir* **2013**, *29* (17), 5230–5238. https://doi.org/10.1021/la400801s.

(82) Doudrick, K.; Liu, S.; Mutunga, E. M.; Klein, K. L.; Damle, V.; Varanasi, K. K.; Rykaczewski, K. Different Shades of Oxide: From Nanoscale Wetting Mechanisms to Contact Printing of Gallium-Based Liquid Metals. *Langmuir* **2014**, *30* (23), 6867–6877. https://doi.org/10.1021/la5012023.

(83) Liu, S.; Sun, X.; Kemme, N.; Damle, V. G.; Schott, C.; Herrmann, M.; Rykaczewski, K. Can Liquid Metal Flow in Microchannels Made of Its Own Oxide Skin? *Microfluid. Nanofluidics* **2016**, *20* (1), 1–6. https://doi.org/10.1007/s10404-015-1665-2.

(84) Goldstein, J. I.; Newbury, D. E.; Michael, J. R.; Ritchie, N. W. M.; Scott, J. H. J.; Joy, D. C. *Scanning Electron Microscopy and X-Ray Microanalysis*; Springer, 2017.

(85) Rajagopalan, M.; Bhatia, M. A.; Tschopp, M. A.; Srolovitz, D. J.; Solanki, K. N. Atomic-Scale Analysis of Liquid-Gallium Embrittlement of Aluminum Grain Boundaries. *Acta Mater.* **2014**, *73*, 312–325. https://doi.org/10.1016/j.actamat.2014.04.011.

(86) Lyon, R. N. *Liquid Metals Handbook, The Committee on the Basic Properties of Liquid Metals*; 1952.

(87) Ndieguene, A.; Albert, P.; Fortin, C.; Oberson, V.; Sylvestre, J. Eternal Packages: Liquid Metal Flip Chip Devices. In *2016 IEEE 66th Electronic Components and Technology Conference (ECTC)*; 2016; pp 580–587. https://doi.org/10.1109/ECTC.2016.29.

(88) Zhao, X.; Liu, J. Liquid Metal Vacuoles. *Adv. Mater. Interfaces* **2022**, *9* (20), 2200583. https://doi.org/10.1002/admi.202200583.

(89) Winsor, P. A. HYDROTROPY, SOLUBILISATION AND RELATED EMULSIFICATION PROCESSES. *Trans. Faraday Soc.* **1948**, *44*, 376–398. https://doi.org/10.1039/tf9484400376.

(90) Kempers, R.; Kolodner, P.; Lyons, A.; Robinson, A. J. A High-Precision Apparatus for the Characterization of Thermal Interface Materials. *Rev. Sci. Instrum.* **2009**, *80* (9), 095111. https://doi.org/10.1063/1.3193715.

(91) Antoniou, N.; Rykaczewski, K.; Uchic, M. D. In Situ FIB-SEM Characterization and Manipulation Methods . *MRS Bull.* **2014**, *39* (4), 347–352. https://doi.org/10.1557/mrs.2014.58.

APPENDIX A

SUPPORTING INFORMATION FOR CHAPTER 2

S1. Preparation of Gallium Foam

Gallium metal (99.99% purchased from Rotometals) was heated on a hot plate between 35 and 40°C to liquify the material. 100 g of liquid gallium was transferred into a plastic 50 mL beaker using a syringe and stirred at 600 rpm using an industrial mixer with a 3D-printed cross-shaped impeller as shown in Fig. S1a. Mixing times for each 100 g batch of liquid metal varies as follows (in minutes): 0, 2, 3.5, 5, 7.5, 10, 15, 30, 60, 90, and 120. While mixing, the liquid metal was kept warm to maintain its liquid state by blowing air from a heat gun. The impeller for mixing the liquid metal was custom designed to fit with the beaker. The fabrication of the impeller was accomplished by a MakerBot Replicator 3D printer using 1.75 mm PLA filament. An isometric view and the dimensions of impeller are shown in Fig. S1b. A high-speed camera (Photron FastCam mini UX-100, Type: 800K-M-16GB with Sigma 18-250 mm F3.5-6.3 DC MACRO OS HSM lens) was used to image the surface of the LM during the mixing at a 45-degree angle (see example consecutive images of surface waves in Fig. S2). The imaging was performed at 4000 frames per second. To provide enough light for high speed imaging, several lamps were mounted around the apparatus.

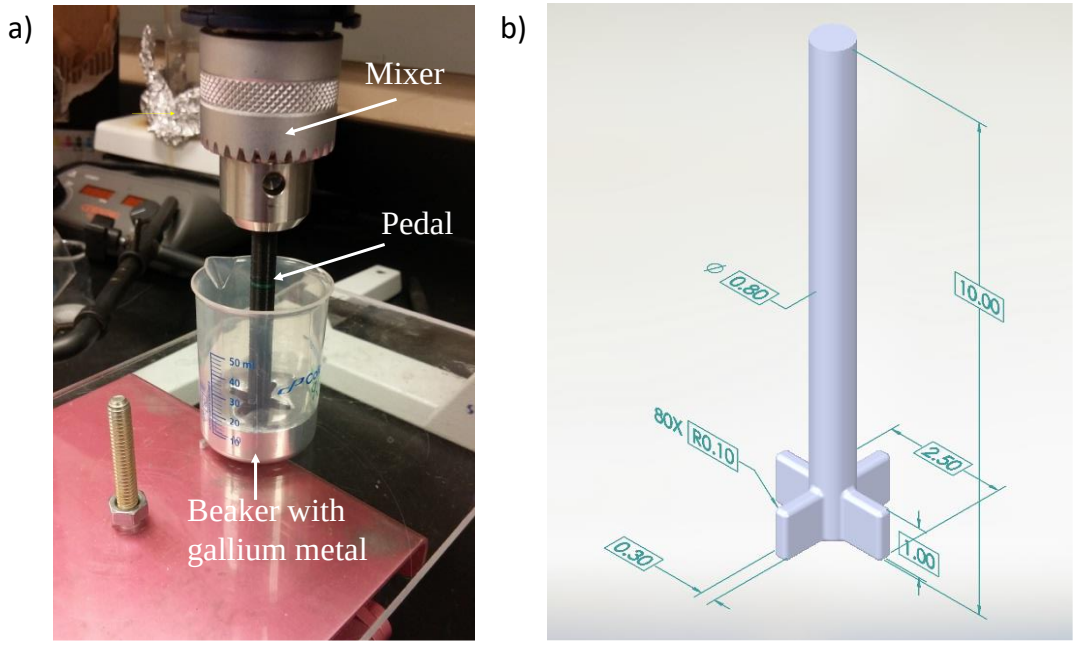

Fig. S1. Setup for preparation of gallium metal foam: (a) mixing arrangement of liquid metal, (b) isometric view of the impeller used for mixing gallium (all the dimensions are in cm). Note that all edges on the cross-shaped impeller have fillets of 0.10 cm radius.

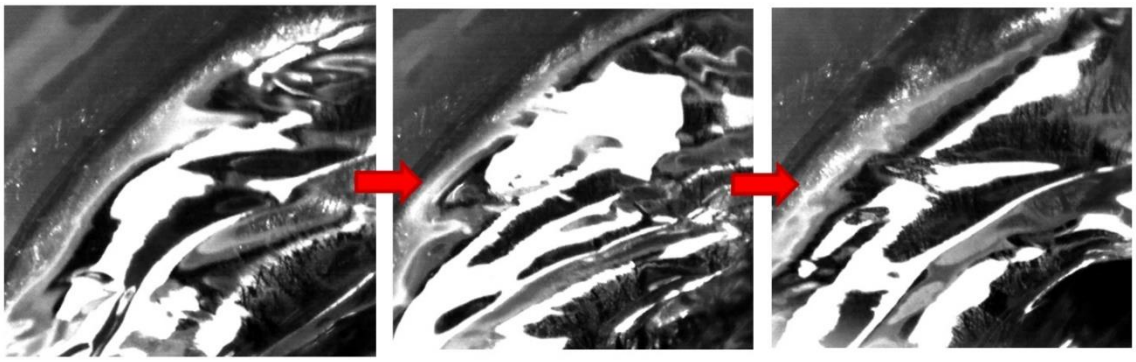

Fig. S2. Consecutive high-speed images of LM surface as the waves and ripples fracture the surface oxides floating on top.

S2. Materials Characterization

Thermal Characterization

The thermal conductivity of gallium foams was characterized using a thermal reference bar testing method following a modified ASTM D5470 standard.[90] The schematic of the testing apparatus is shown in Fig. S4a. The LM-foam was applied onto the copper reference bar and compressed to a 1.5 mm thickness and ~0.1 MPa for each measurement. A Teflon gasket was used to keep the LM-foam in place while testing. Please note that the low-density foam in the prepared samples mixed at shorter times tend to rise from the bulk LM, causing stratification. Effort was made to minimize the effect of stratification by rapidly stirring the sample to homogenize the sample before applying onto the reference bar. During the measurement, the samples were at about 70 to 75 °C.

Density Characterization

The density of each gallium foam sample was determined following the Archimedes principle.[54] A circular disk of gallium samples (2 cm diameter and 6 mm thick) is cast using a polymer mold and the buoyant force is measured by suspending the disk in a 50 mL beaker of water on a microbalance as shown in Fig. S4b.

Rheological Characterization

All rheological experiments conducted for this report were performed with a TA AR-G2 rotational rheometer. A parallel plate of 40 mm diameter and a gap height of 800 μm were used as the geometry for the rheological experiments. The upper plate was attached with sandpaper and the liquid metal was placed on a petri dish attached on the bottom plate

to avoid metal-metal contact with the liquid metal samples. All tests were performed at 40 °C, which is above the melting temperature of gallium, to avoid the liquid metal from solidification. Two tests were performed to measure the storage modulus and viscosity of the samples including oscillatory frequency sweep test and flow sweep test. Oscillatory frequency sweep test was performed at 2% strain with a frequency sweep from 0.1 to 100 rad/s. Flow sweep test was performed by varying the shear rate from 0.1 to 100 s^{-1}. The error bars shown represent the standard deviation between multiple samples and across a range of angular frequencies (0.1 to 100 $rad.s^{-1}$).

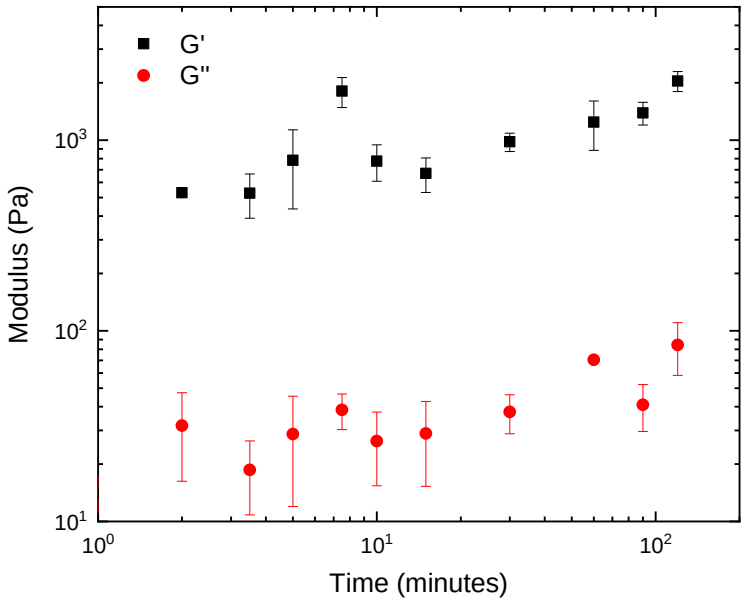

Fig. S3. Comparison of the storage and loss modulus of the liquid metal at increasing mixing times.

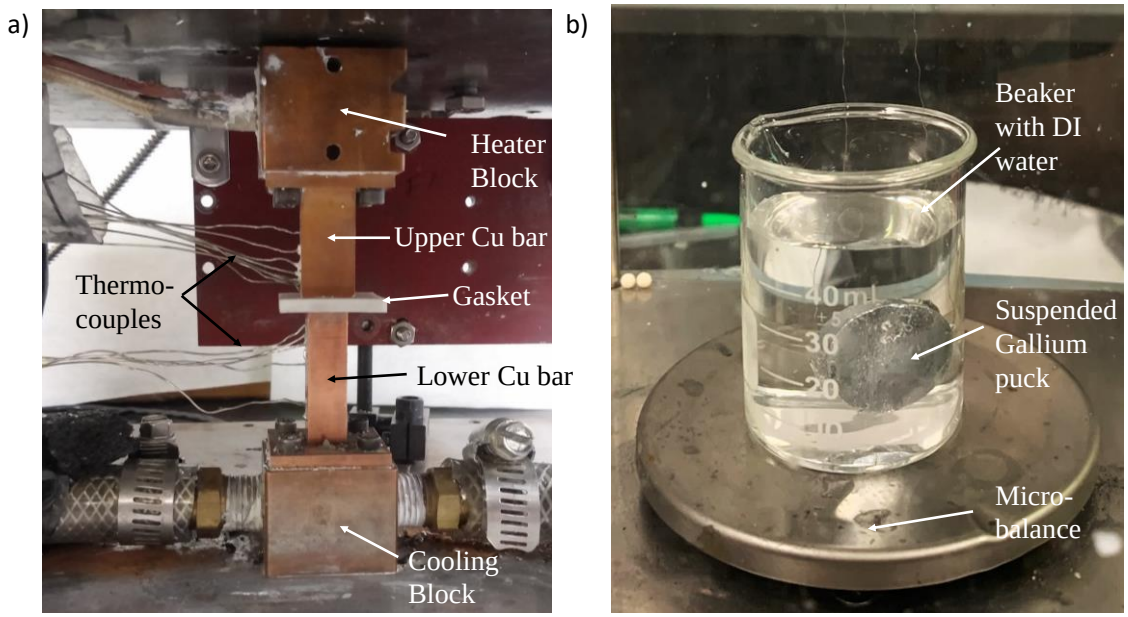

Fig. S4. Characterization of gallium foams (a) schematic of thermal conductivity testing apparatus; (b) schematic of density measurement using Archimedes' method.

S3. Cross-Sectioning of Oxide Flakes

Microscopic images were collected with an Amray 1910 FESEM with 20 kV accelerating voltage. Cross sections of imaged frozen sample blocks (at room temperature) were prepared by cleaving the surface with a razor blade edge. A focused ion beam (FEI NOVA 200 FIB-SEM) with a gallium ion column is used to cross section small sections of gallium stirred in air and show the crumpled oxide flakes within (Fig. S5). Cross sections of larger samples were cleaved manually with a razor blade. Higher magnification SEM images of solidified gallium cross sections mixed at various times is shown in Fig. S6.

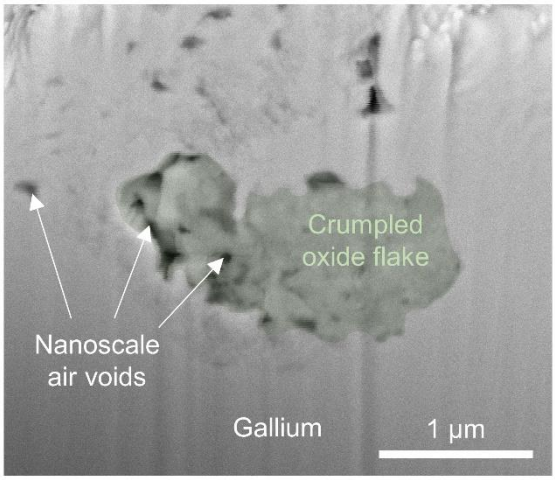

Fig. S5. Cryogenic Focused Ion Beam-Scanning Electron Microscope cross-sectional image of a crumpled oxide flake (colored in light green) in a gallium foam that was stirred for ~5 minutes. The milling and imaging processes were performed using our typical procedure, that is described in detail elsewhere.[53,91]

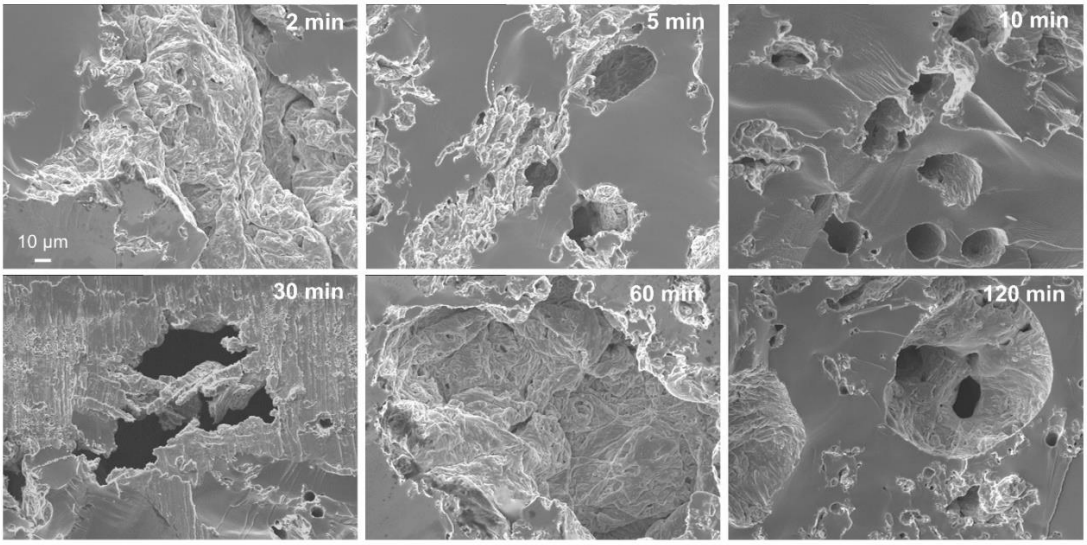

Fig. S6. SEM images of solidified gallium foam cross sections at high magnification.

S4. Expanded Results

Fig. S7 shows the density data which is used to calculate the mean density as in Fig. 2b of the main text. It can be noted that for density measurement, three LM-foam pucks were made corresponding to each stirring time. Fig. S8 shows the total data points collected for thermal conductivity. For each LM-foam sample, at least five thermal tests were performed. The error bars in Fig. 2c represent the standard deviation from the averaged standard deviations of each individual data point shown here. The storage modulus of the different LM-foam samples is plotted against the porosity (Fig. S9) which is calculated from the ratio of the average density of each sample to the density of the pure gallium sample.

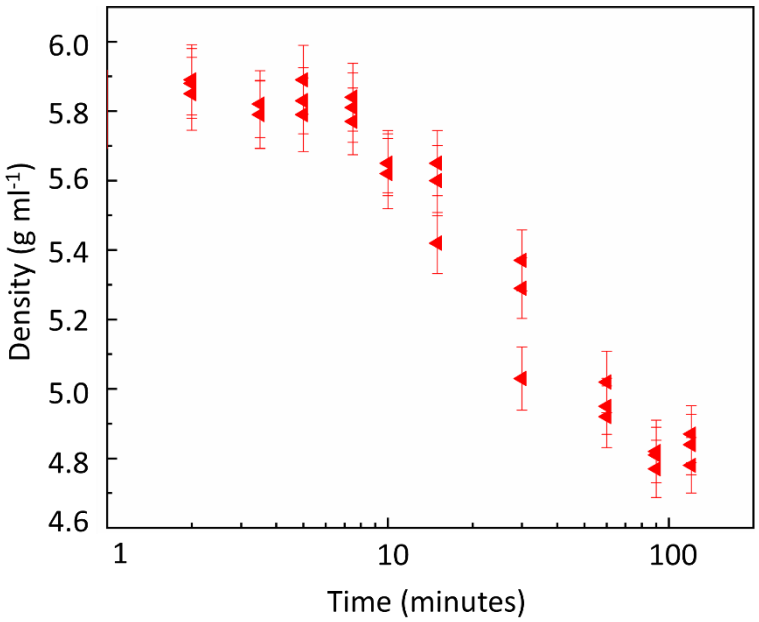

Fig. S7. All collected LM foam density data.

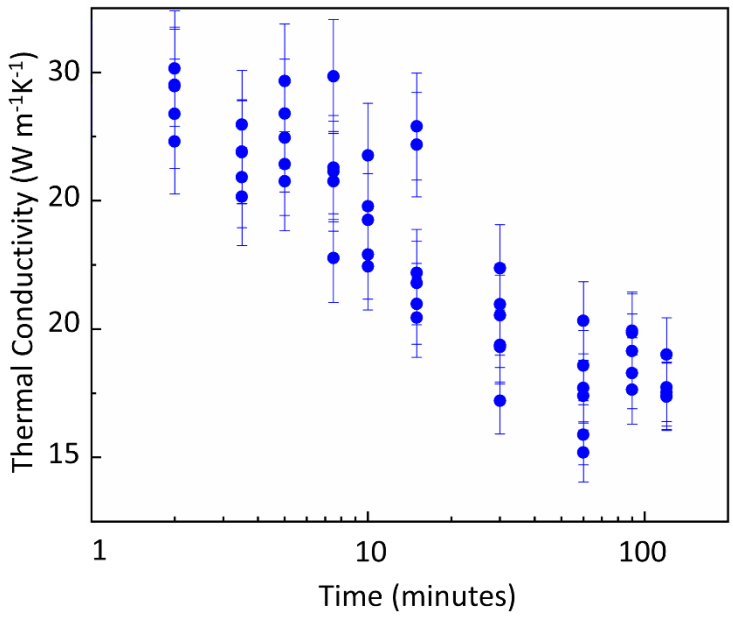

Fig. S8. All collected LM foam thermal conductivity data.

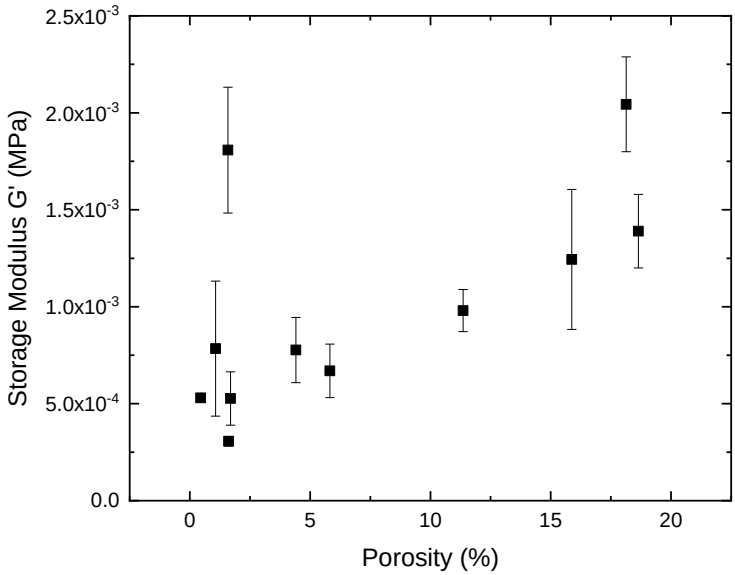

Fig. S9. Storage modulus vs calculated gallium foam porosity.

APPENDIX B

SUPPORTING INFORMATION FOR CHAPTER 3

S1. LM-in-oil droplet size distribution for various mixing times

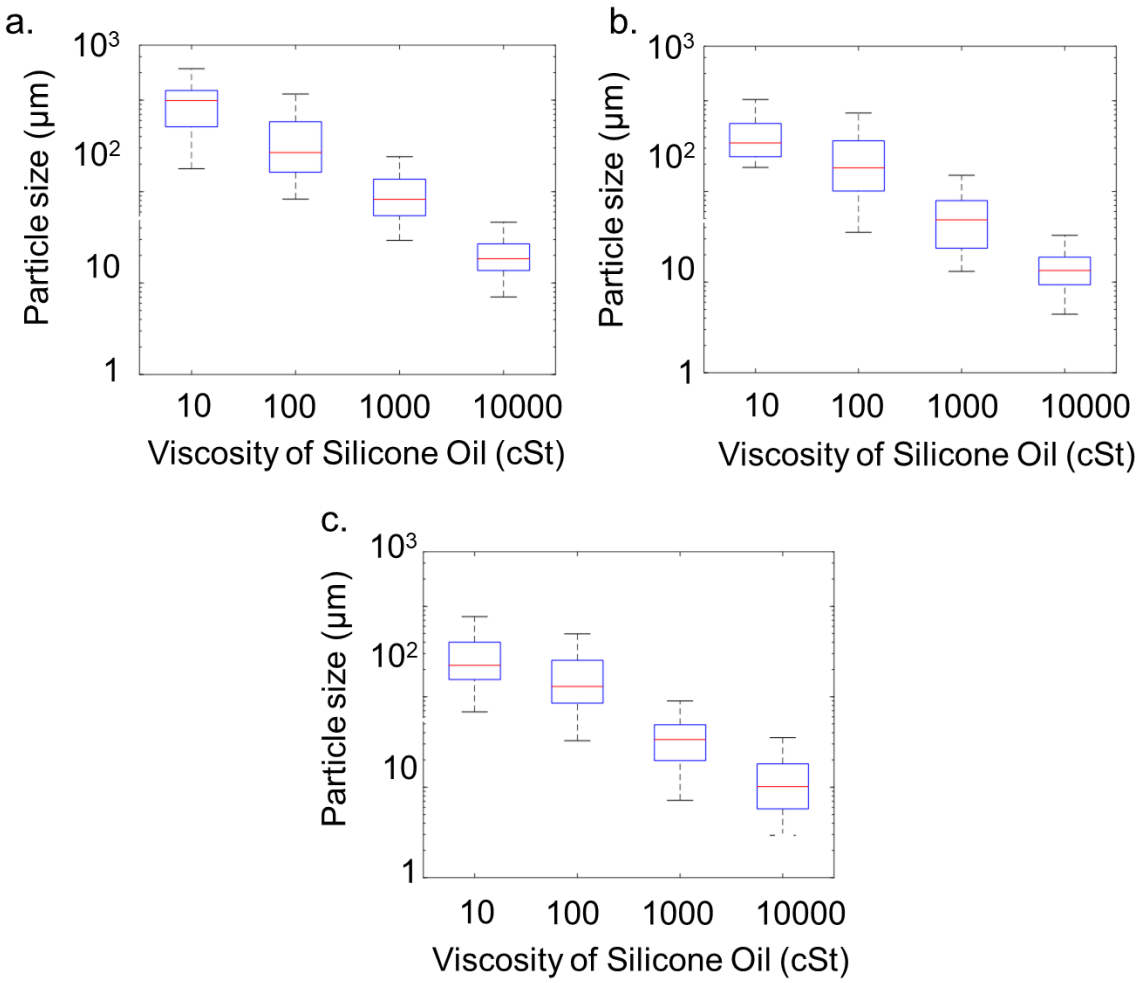

Figure S3. Size distribution of LM particles in LM-in-oil emulsion at 20:80 SO:LM volume ratio against the viscosity of used silicone oil (SO) after manual mixing 120 minutes for (a) 10 minutes, (b) 30 minutes and (c) 60 minutes. In the box plots, red bar correspond to median, blue box represents inter-quartile range (Q1-Q3) and the black extending lines (whiskers) represent the range of particle size.

S2. 7-day corrosion test results

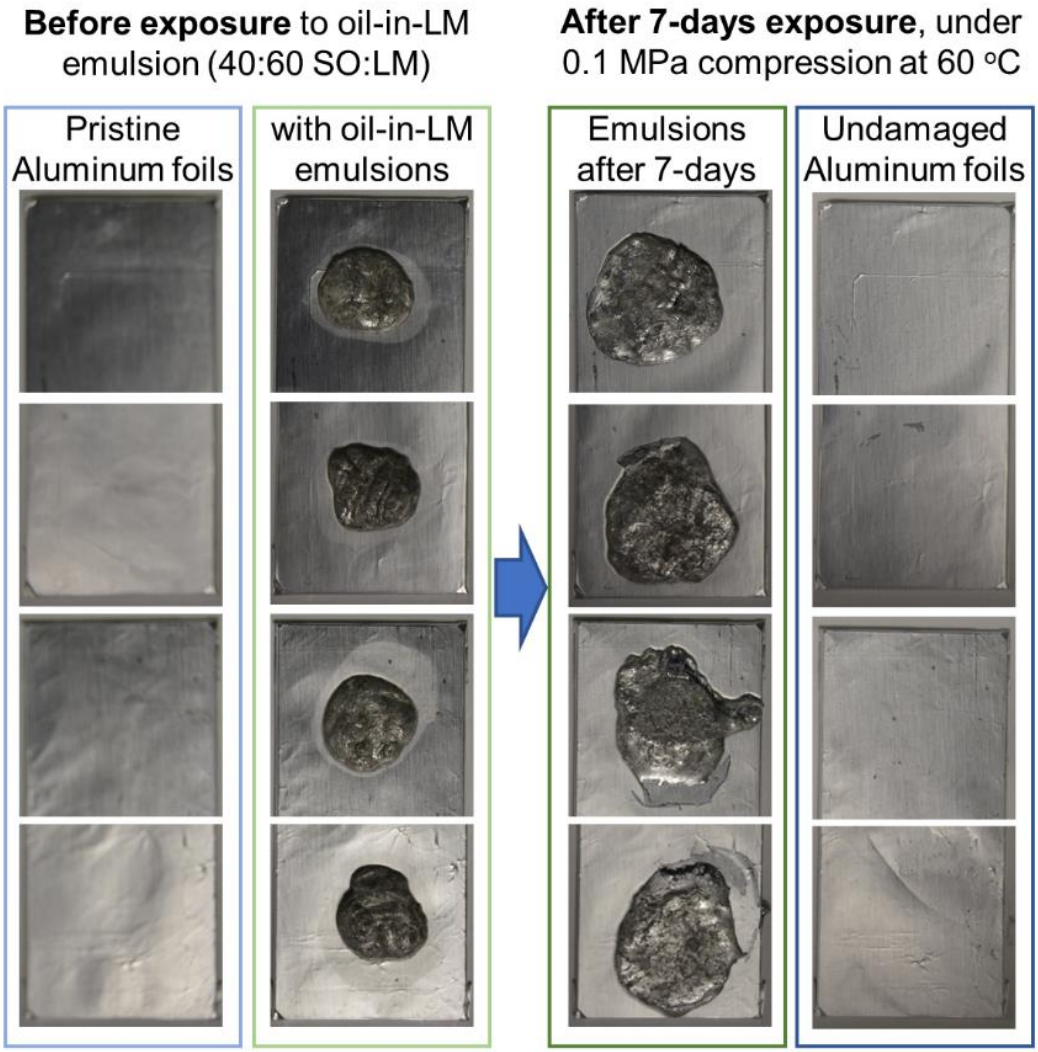

Figure S4. Corrosion resistance characteristic of the oil-in-LM emulsion (40:60 SO:LM) illustrated by exposing aluminum foil to the emulsion samples for 7-days under 0.1 MPa applied pressure and at 60 ^{o}C.

APPENDIX C

SUPPORTING INFORMATION FOR CHAPTER 4

S1. Scalable Fabrication of Silicone Oil in Liquid Metal Emulsions by high rate stirring

Silicone oil-in-Liquid Metal (SO-in-LM) emulsions may also be prepared using an industrial mixer (see our prior work for further details[30,71]). **Figure S1(a)** demonstrates the mixing of SO and *a priori* made LM foam using a stainless-steel stirrer (removed from Orment Led Lighting Epoxy Resin Electric Mixer) at 2000 rpm for 2 minutes.

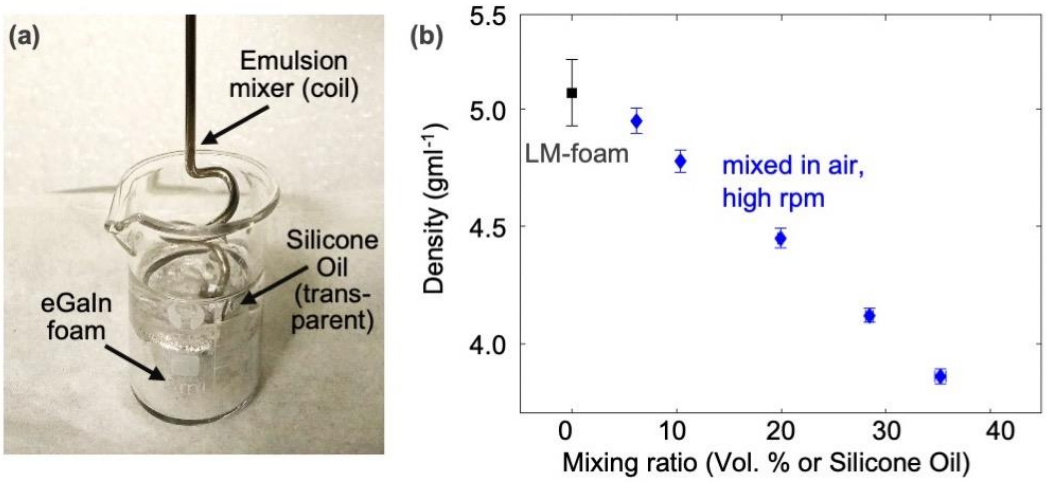

Figure S2. (a) Setup for preparation of SO-in-LM emulsions by high rate stirring, **(b)** the density of the resulting SO-in-LM emulsions as a function of volume percentage of SO. The data values and trends in this data set are similar to the data in Figure 4.2 of chapter 2, albeit with minor differences due to a difference in mixing method.

S2. Estimated Internalized Volume in the SO-in-LM emulsions

After the silicone oil and LM foam mixing processes, some excess oil can remain on in the mixing vessel or the mixing rod. While difficult to measure exactly, **Figure S2** presents estimates of actual volume of silicone oil incorporated into LM foam for each of

the discussed experiments that was obtained using additional mass measurements of the rod and the mixing vessel before and after the emulsion fabrication process.

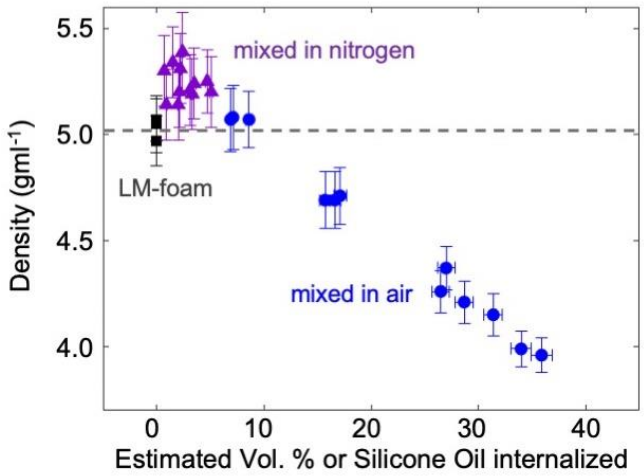

Figure S3. Plot of density as a function of estimated volume of silicone internalized into the LM foam during mixing in air or nitrogen environments.

S3. Effect of Viscosity of Silicone Oil and LM foam Mixed in a Nitrogen Environment

LM foam was mixed with the different viscosities (10, 100 and 1000 cSt) of SO in a nitrogen environment. In all cases, the majority of the SO does not internalize into the LM foam as shown in **Figure S3**. In the case of a higher viscosity of 1000 cSt, the LM-foam disperses into smaller droplets in the SO over the course of mixing.

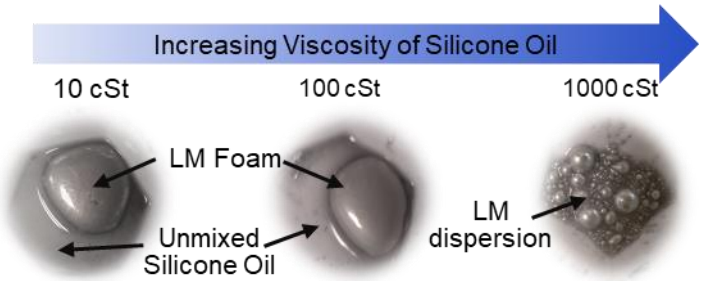

Figure S4. The results of mixing LM foam with different viscosities of silicone oil in a nitrogen environment.

S4. Mixing of peroxide with the LM foam

In contrast to the SO (which does not mix with the LM foam in a nitrogen environment), an oxidizing fluid such as 10% w/w hydrogen peroxide (H_2O_2) readily internalizes in the LM foam resulting in a H_2O_2-in-LM emulsion. The internalization of H_2O_2 into LM foam in air and nitrogen occur in approximately the same amount of mixing time. It is also noted that oxidation of Ga using H_2O_2 may release hydrogen gas, this may be observed by some swelling of the LM Foam during the mixing process. Furthermore, caution must be taken in this process to prevent hydrogen from spontaneous reaction in air.

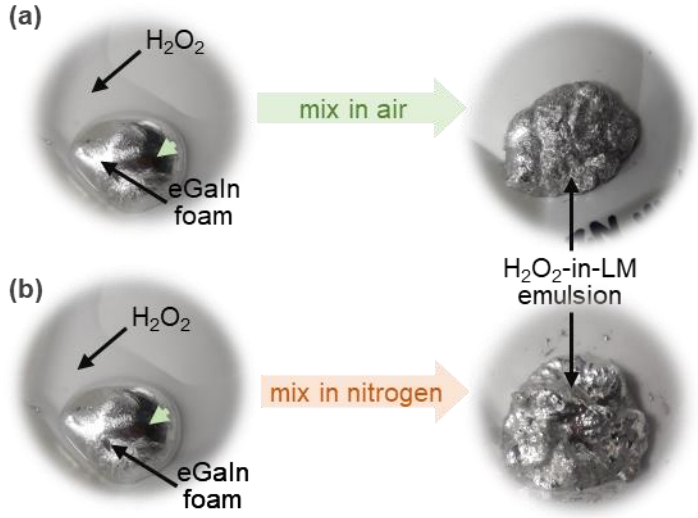

Figure S5. Mixing of LM foam with hydrogen peroxide in **(a)** air and in a **(b)** nitrogen environment

S5. Cross-sectional images of SO-in-LM emulsions

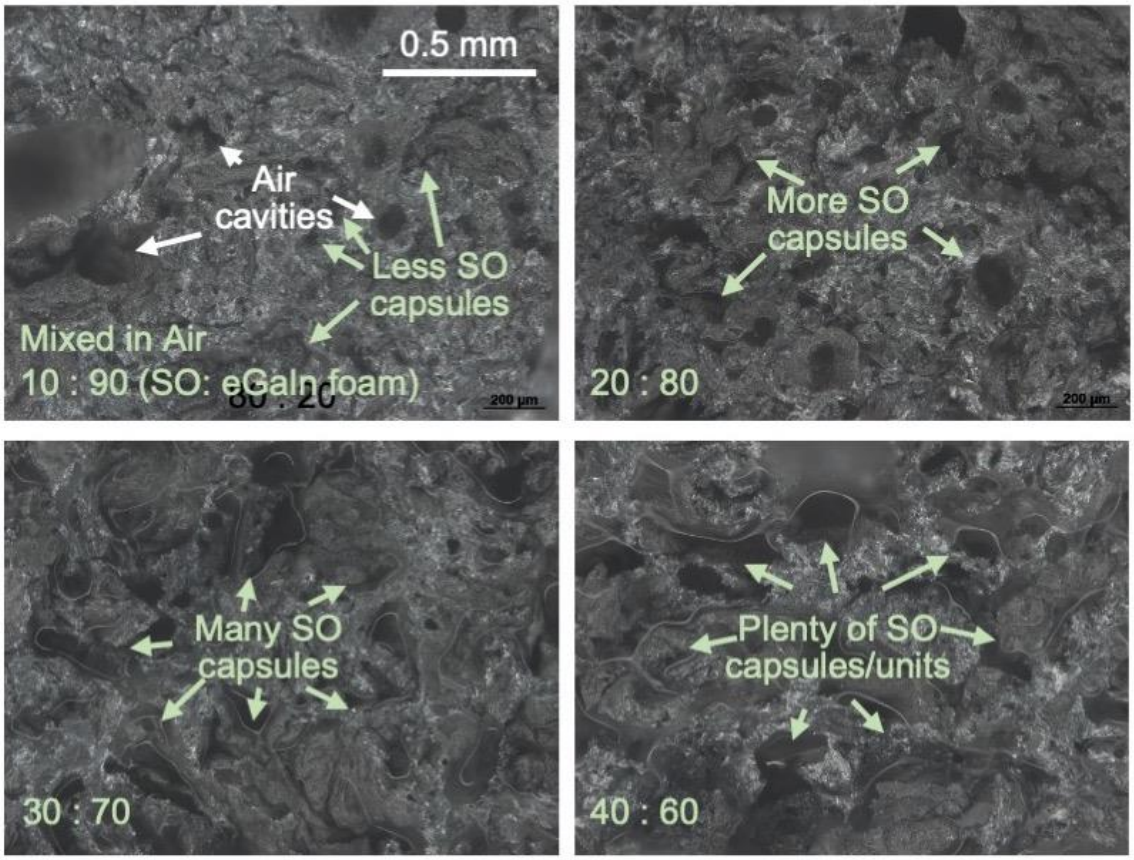

Figure S6. Optical microscope image of cross-sections of SO-in-LM emulsions resulting from mixing in air for SO to LM foam volume ratios ranging from 10:90 to 40:60.

S6. Testing of LM induced aluminum embrittlement of the SO-in-LM emulsions and SO mixed with LM foam in nitrogen

Gallium-induced embrittlement of aluminum by the emulsions and mixtures made in nitrogen environments was tested using the procedure in my prior work[2] that consists of compressing the LM-material in-between two aluminum foils for 24 hours (see schematic and images in **Figure S6a-b**).

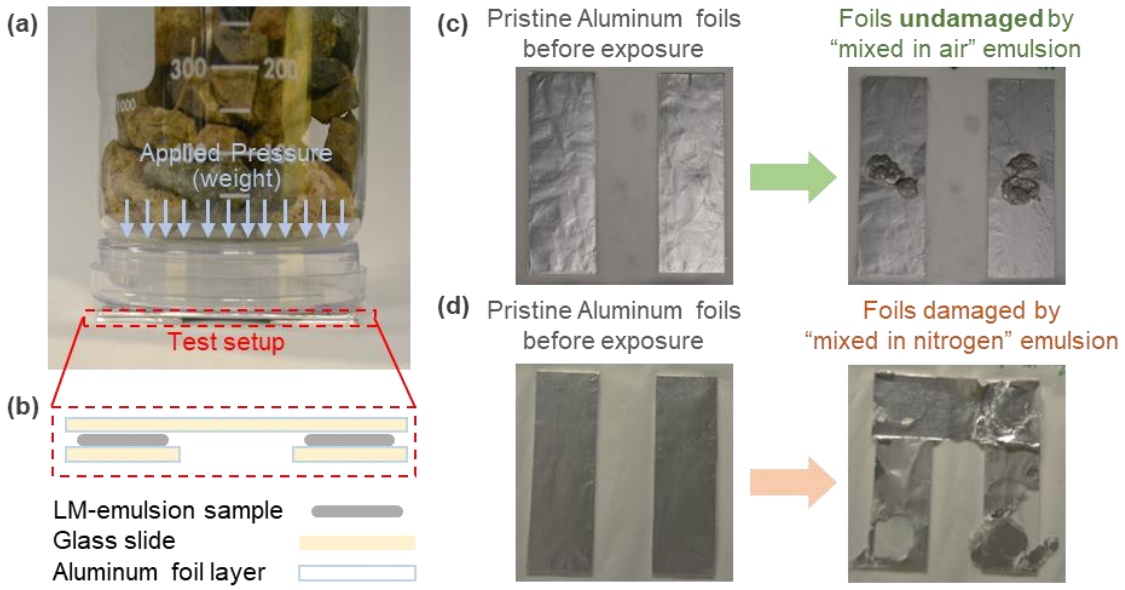

Figure S6. Testing of LM induced corrosion of SO-in-LM Emulsion and SO mixed with LM foam in a nitrogen environment: **(a)** actual test setup consisting the LM samples sandwiched between a set of glass-slides covered by Aluminum foils, while external pressure is applied, **(b)** expanded schematical view of the test setup, **(c,d)** images showing pristine aluminum foils before and after exposure to the **(c)** SO-in-LM emulsion (made in air) and that **(d)** SO mixed with LM foam in a nitrogen environment.

BIOGRAPHICAL SKETCH

Najam Ul Hassan Shah was born in 1988 in a countryside of district Faisalabad of Pakistan. He grew up with his parents and completed all his education up to masters in his home country, Pakistan. During his childhood, he accompanied his parents to different places across the country due to his father's job. He attended several different schools before finally completing his secondary and intermediate education in 2004 and 2006 respectively from Kamalia city, which later became his hometown. Najam's family then moved to Burewala for a period of six years. During this time, he attended the University of Engineering and Technology (UET) Lahore, a public sector university in Pakistan as an undergraduate student in mechanical engineering. His undergraduate final year project focused on solar energy storage by a salinity-gradient solar pond. After graduating from UET Lahore in 2012, Najam moved to Karachi and worked at Eni Pakistan Limited as a graduate trainee for one year. After this first job, his interest in higher education led him to explore career in education sector. In fall of 2014, he joined mechanical engineering faculty of UET Taxila as a Lab Engineer, while simultaneously finding admission in their master's program in mechanical engineering. He worked under the supervision of Dr. Muzaffar Ali, an expert in HVAC, thermal and renewable energy, for his master's thesis titled "performance analysis of phase change material based thermal energy storage for concentrated solar plant". Najam moved to Arizona State University (ASU) in 2018 to pursue his PhD in mechanical engineering funded by the prestigious Fulbright-HEC scholarship program. At ASU, he shifted his research focus to liquid metal-based foams and emulsions. His thesis was co-advised by Dr. Robert Wang and Dr. Konrad Rykaczewski. After completing his PhD, Najam will be joining back the mechanical engineering faculty of UET Taxila, Pakistan. As of today, Najam has authored a total of six peer-reviewed articles including one manuscript under review.